Probing the nature of electroweak symmetry breaking with Higgs boson pair-production at ATLAS

Shahzad Ali
on behalf of the ATLAS Collaboration

14th Conference on the Intersections of Particle and Nuclear Physics
(CIPANP 2022)

30/08/2022

Higgs self-coupling measurements at the LHC

- The trilinear Higgs coupling (λ_{HHH}) directly accesses the shape of the scalar potential and thus direct test of the EW symmetry breaking
- Higgs pair (HH) productions at LHC provides a direct probe to the measurement λ_{HHH}

$$V(H) = \frac{1}{2}m_H^2 + \lambda_{HHH}\nu H^3 + \frac{1}{4}\lambda_{HHHH}H^4 - \frac{\lambda}{4}\nu^4$$

$$\lambda_{HHH} = \lambda_{HHHH} = \frac{m_H^2}{2\nu^2} \approx 0.13 \rightarrow \text{SM prediction}$$

Leading HH production mode at LHC is gluon-gluon Fusion (ggF): $\sigma_{ggF}^{SM} = 31.05fb$ at NNLO for $\sqrt{s} = 13$ TeV!

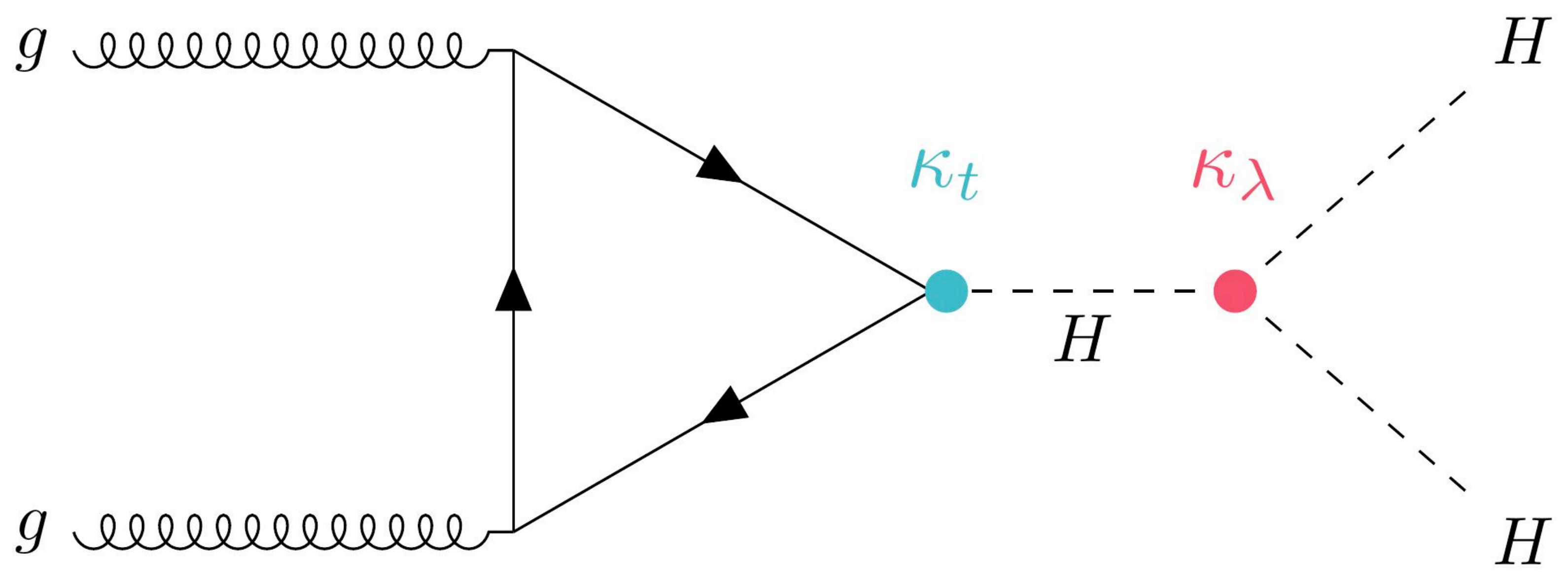

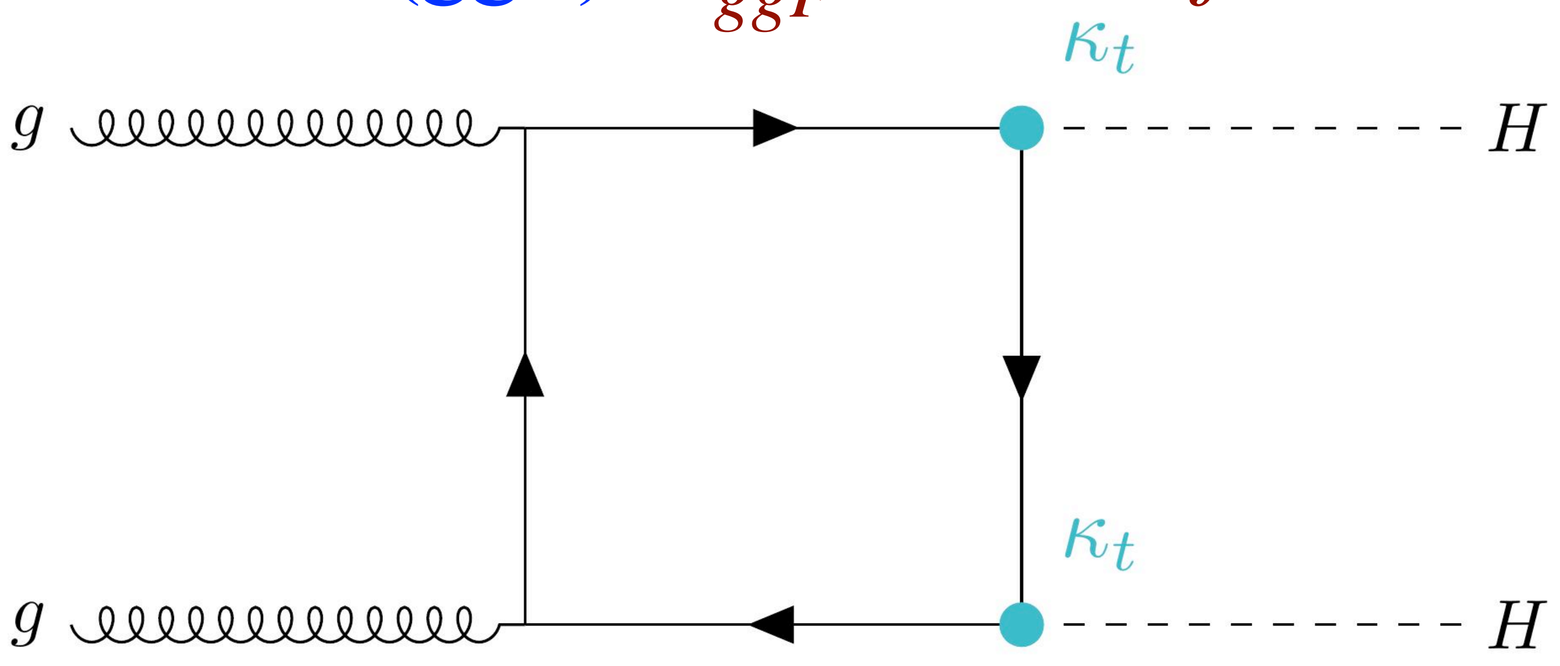

$$\kappa_\lambda = \frac{\lambda_{HHH}^{Measured}}{\lambda_{HHH}^{SM}}$$

Second leading HH production mode is vector-boson-fusion (VBF): $\sigma_{VBF}^{SM} = 1.73fb$ at N3LO for $\sqrt{s} = 13$ TeV!

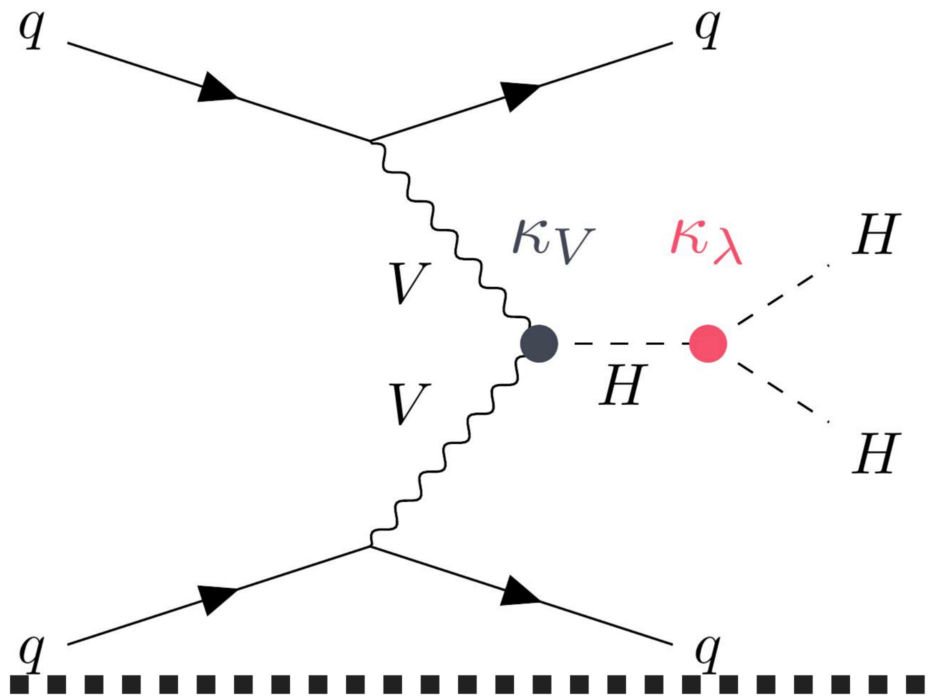

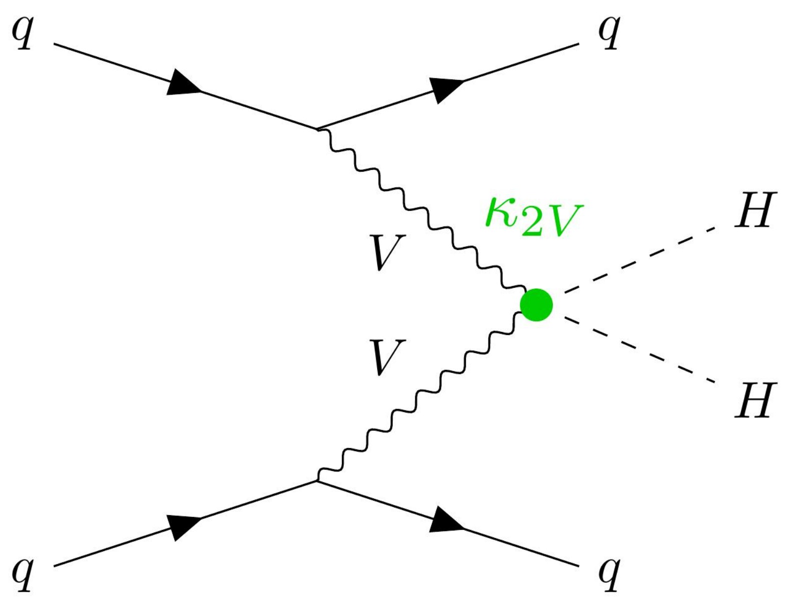

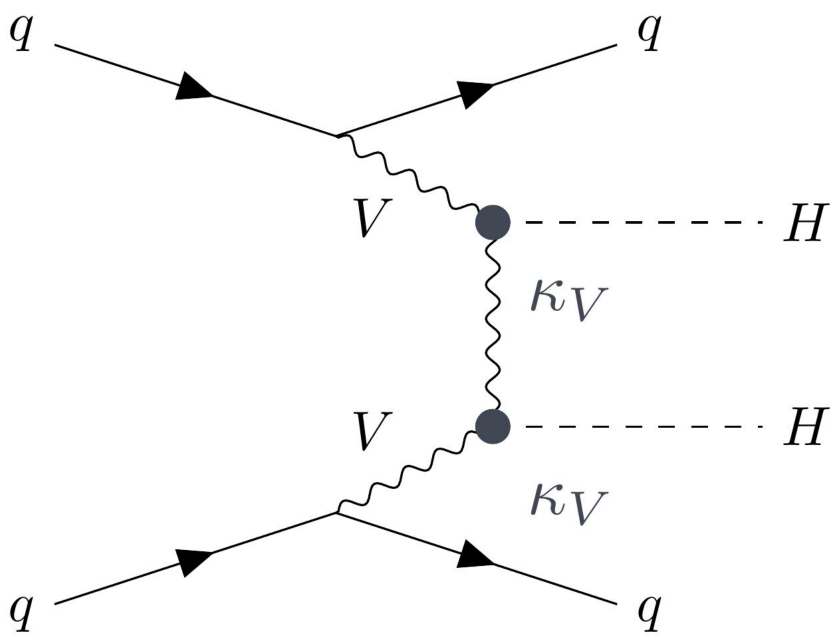

BSM Physics in Higgs pair production

- Higgs pair production in SM is a rare process
  - The production cross-section is 1000 × smaller than the single Higgs production
- But still very interesting to study beyond the SM physics (BSM)

- Large variations of non-resonant cross section with modifications of κ_λ for ggF and VBF
  - More than a factor of 2 increase at $\kappa_\lambda = 0$
  - More than a factor of 4 increase at $\kappa_\lambda = -1$
- Modifications of the kinematics of the process with variations of
  - due to different contributions and interference of the Feynman diagrams

JHEP04(2013)151

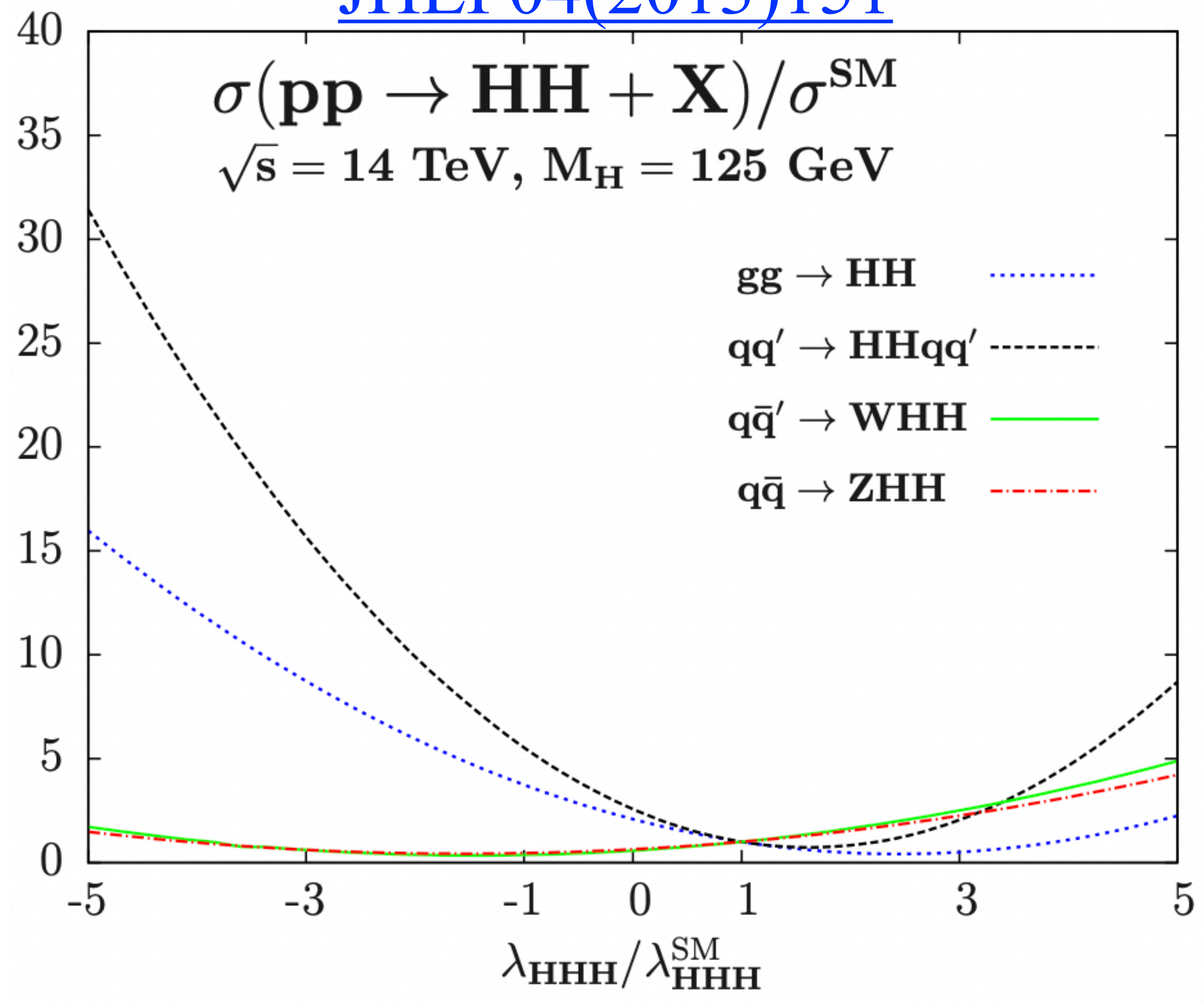

Phys. Lett. B 800 (2020) 135103

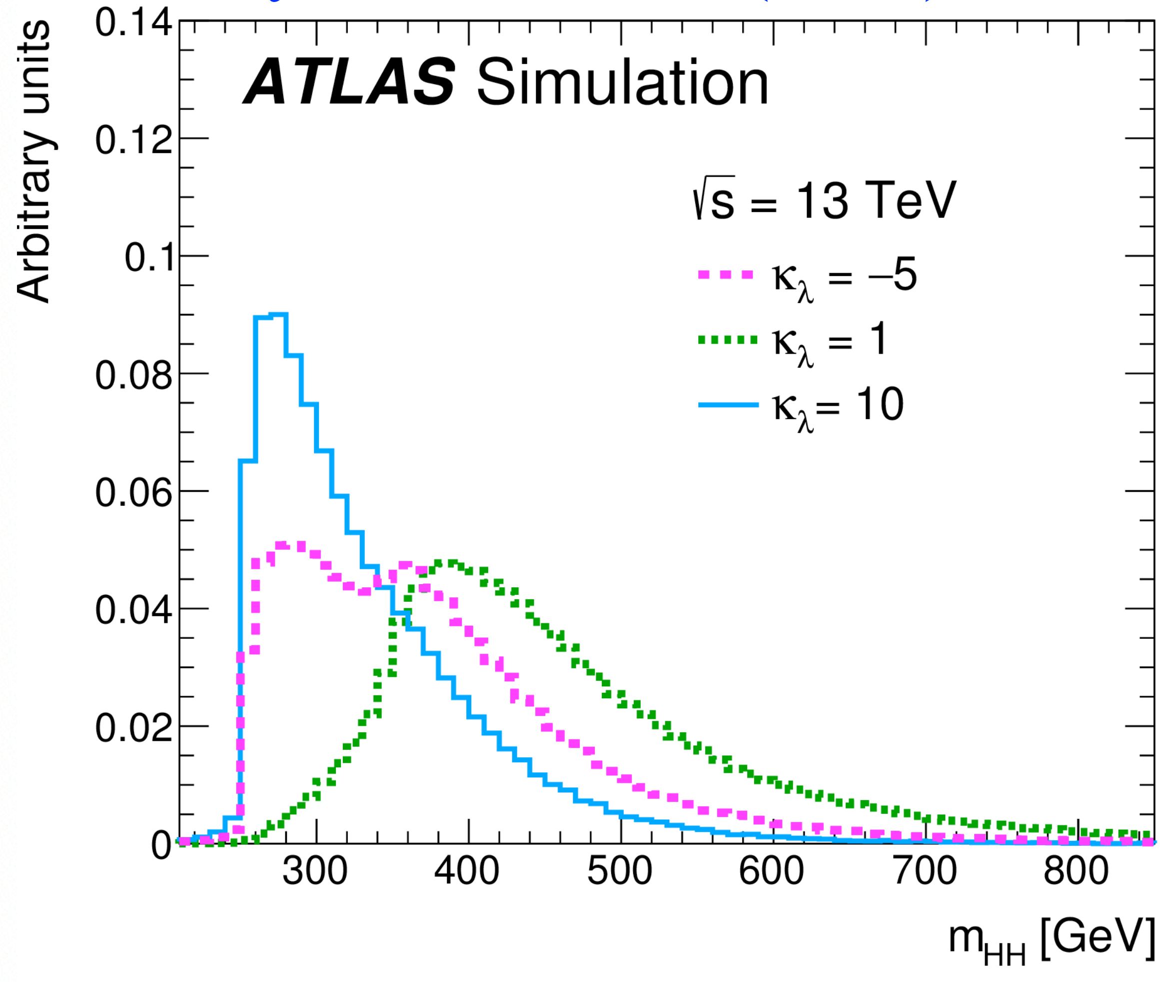

Production of BSM resonances $X \to HH$

- Enhances the production rate

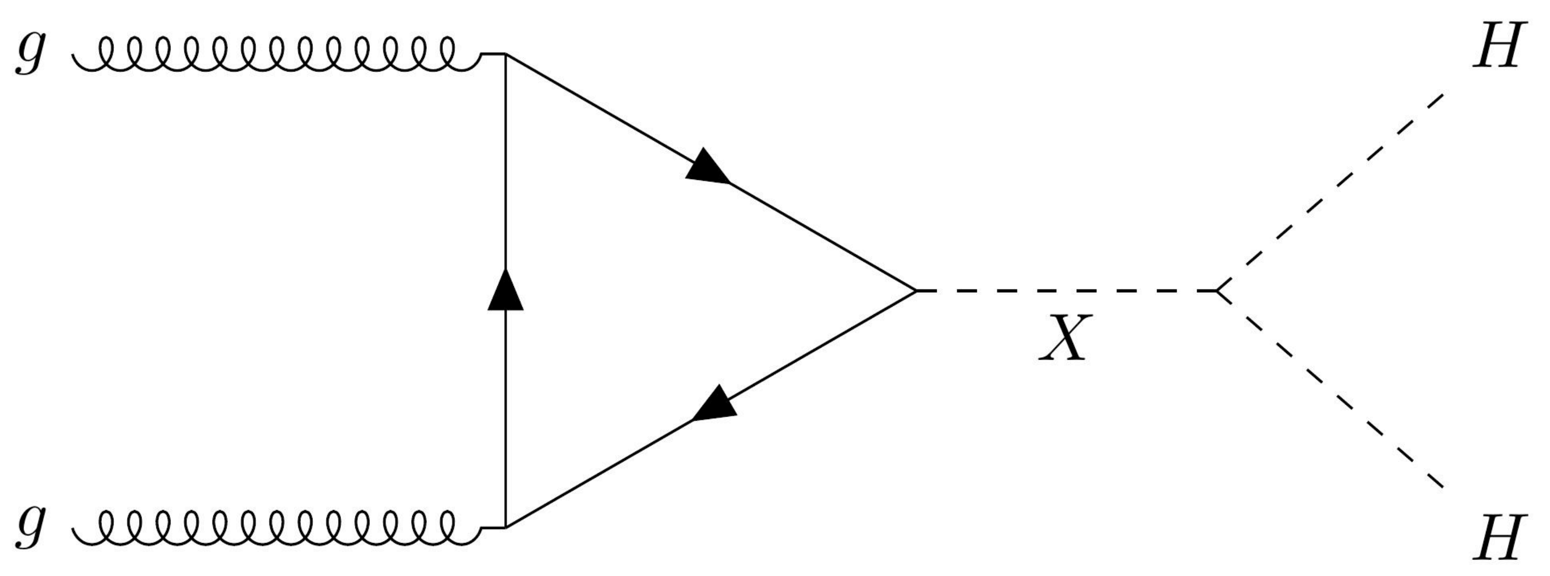

HH decay channels and ATLAS quest for HH production

- Many different final states in the Higgs pair decay given by all possible combinations of Higgs Boson decays
- ATLAS experiment is covering a vast variety of these decay channels and obtained results for $36fb^{-1}$ and full $139fb^{-1}$ LHC Run2 datasets

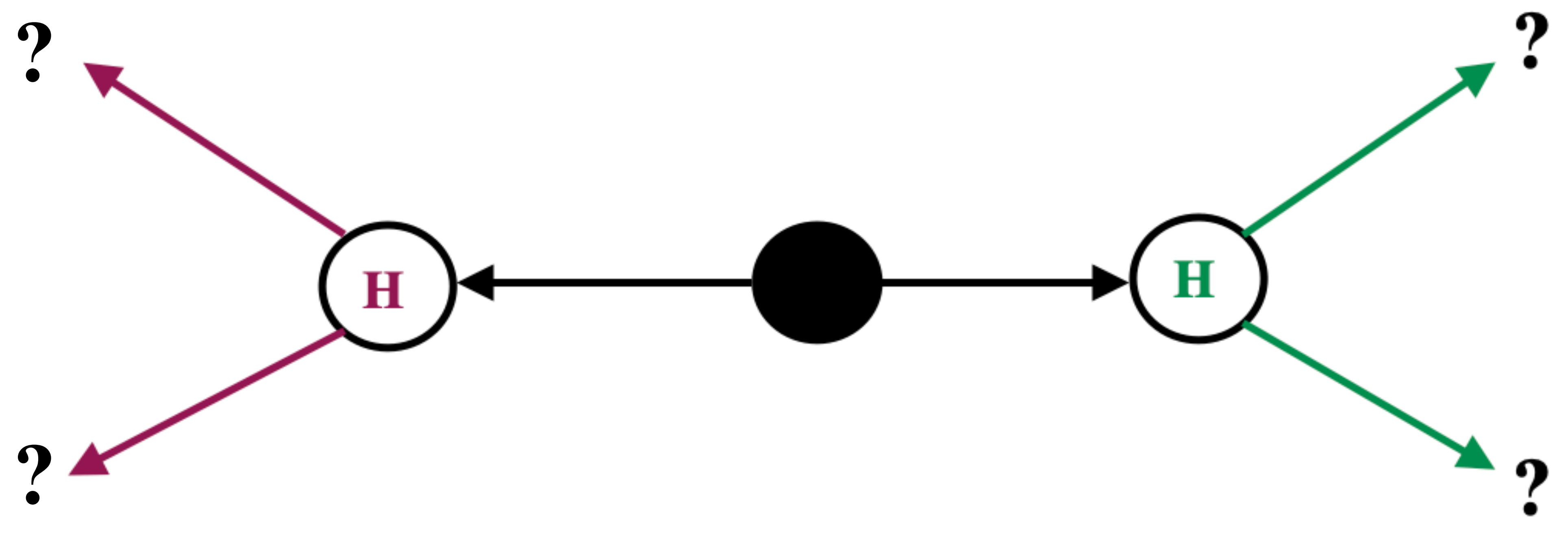

	bb	WW	ττ	ZZ	γγ
bb	34%				
WW	25%	4.6%			
ττ	7.3%	2.7%	0.39%		
ZZ	3.1%	1.1%	0.33%	0.069%	
γγ	0.26%	0.10%	0.028%	0.012%	0.0005%

Given that $H \rightarrow bb$ has the highest B.R is mostly exploited by the searches

- Analyses in different decay channels have very different characteristics given the different signal decay BRs, different objects in the final state and different backgrounds

Will cover the latest ATLAS HH analyses and results for the three most prominent channels using LHC Run2 data: $bbbb$, $bb\tau\tau$, $bb\gamma\gamma$

Non-resonant HH production searches at ATLAS

Full Run2 data results for non-resonant $HH \to bbbb$

ATLAS-CONF-2022-035

- HH → 4b has the largest BR (34%)
- Due to large QCD the multi-jet background make it challenging to distinguish signal from the background
- Search is performed for SM and BSM non-resonant HH production
- Both ggF and VBF HH production mode are considered
- HH → bbbb: at least 4 b-tagged central jets

- Targeting ggF and VBF production modes with dedicated categories based on the presence of additional jets
- Minimum ΔR constraint is implemented on b-jets to form the Higgs candidates
- Signal regions are defined by the selections in the 2D m_{H1}:m_{H2} plane

ggF

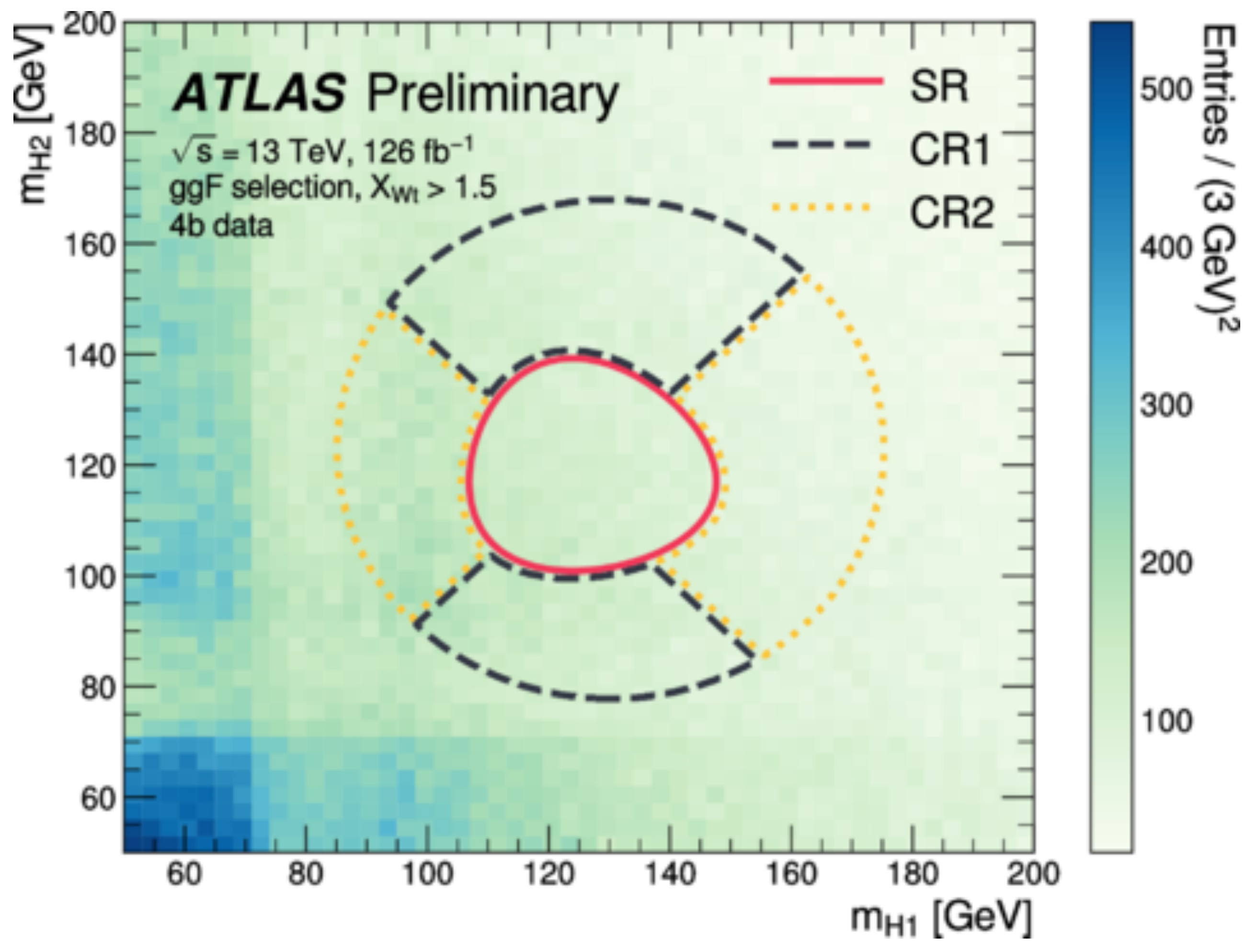

VBF

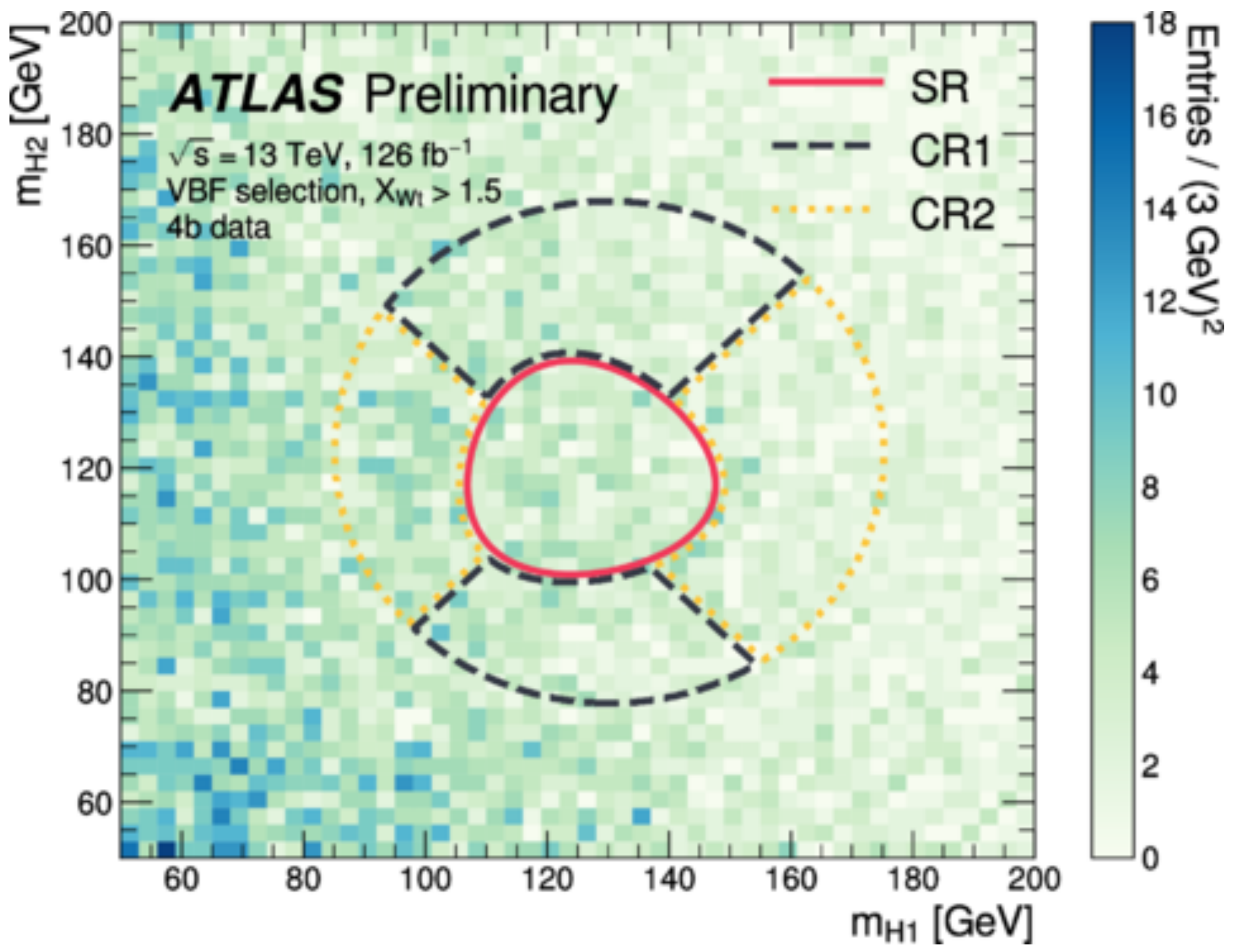

- Major backgrounds
  1. QCD multi-jets (~95 %)
  2. ttbar (~5%)
- Total background estimated from data using a neural network trained in control regions to re-weight 2b data to look like 4b data

Full Run2 data results for non-resonant $HH \to bbbb$

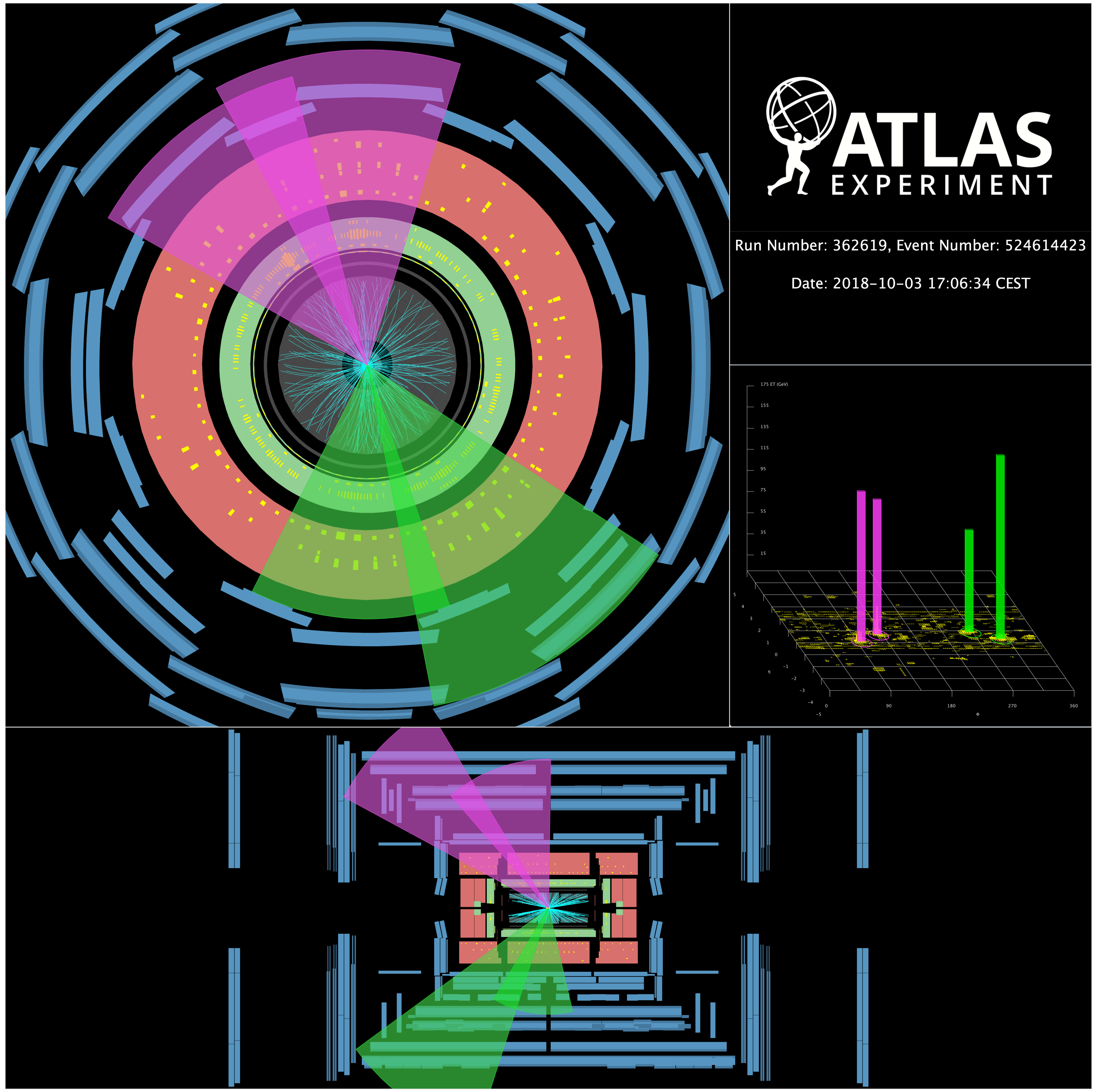

Event display for HH candidate for ggF process

$m_{HH} = 588\,\text{GeV}$ $m_{bb} = 126\,\text{GeV}$ and $m_{bb} = 114\,\text{GeV}$

Full run2 data results for non-resonant $HH \rightarrow bbbb$

- Further splitting is performed for ggF and VBF categories to enhance sensitivity to SM signal and to the signals with BSM couplings
  - ggF category splitting:
    - 3×2 categories in bins of
      - $|\Delta\eta_{HH}| \times X_{HH}$
  - VBF category splitting:
    - 2 categories in bins of
      - $|\Delta\eta_{HH}|$
  - Final discriminant variable:
    - m_{HH} is used as final discriminant variable in the 8 signal regions

$$X_{HH} = \sqrt{\left(\frac{m_{H1} - 124\ \text{GeV}}{0.1\ m_{H1}}\right)^2 + \left(\frac{m_{H2} - 117\ \text{GeV}}{0.1\ m_{H2}}\right)^2}$$

ATLAS-CONF-2022-035

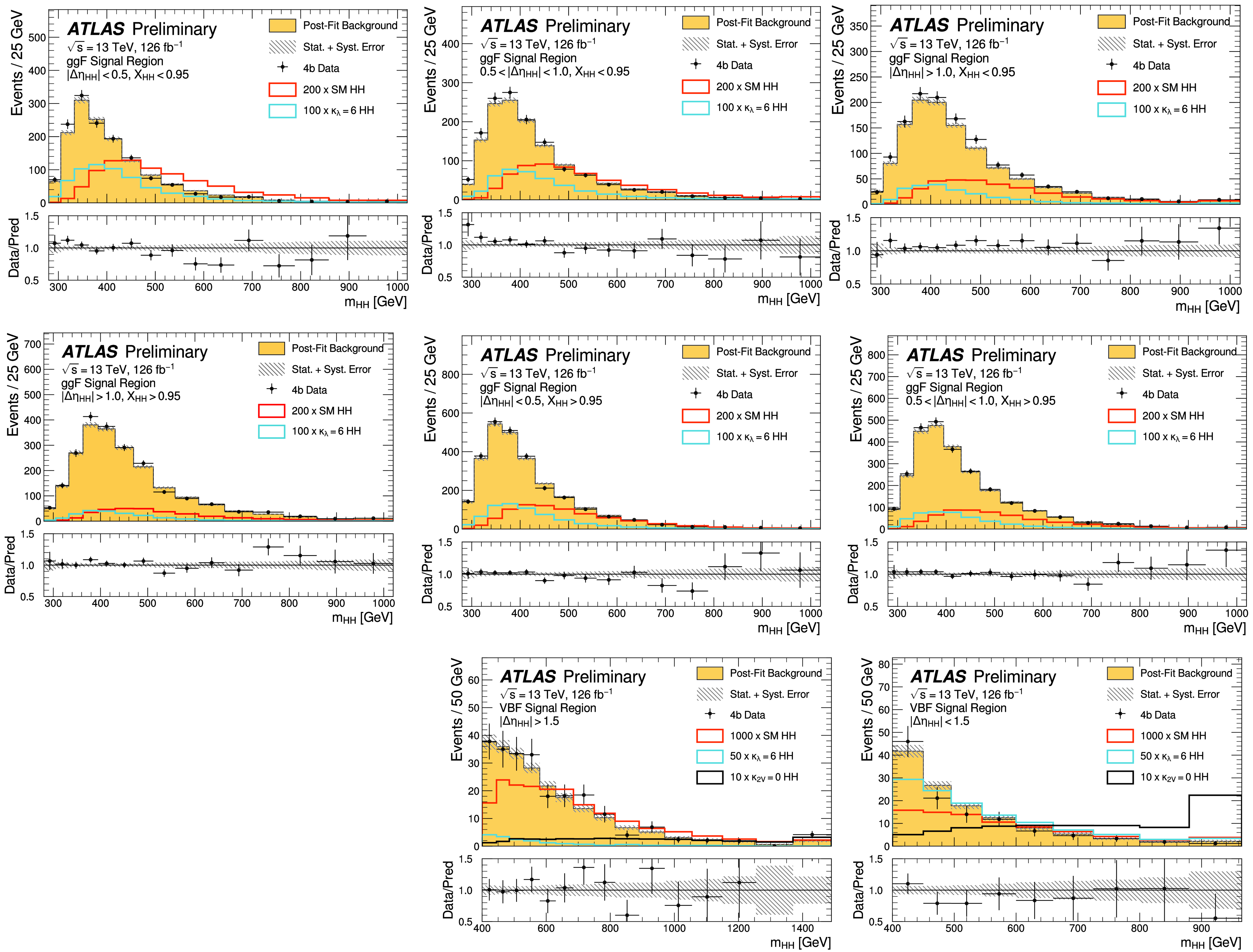

Full Run2 data results for non-resonant $HH \to bbbb$

	Observed Limit	-2σ	-1σ	Expected Limit	$+1\sigma$	$+2\sigma$
$\sigma_{\mathrm{ggF}}/\sigma_{\mathrm{ggF}}^{\mathrm{SM}}$	5.5	4.4	5.9	8.2	12.4	19.6
$\sigma_{\mathrm{VBF}}/\sigma_{\mathrm{VBF}}^{\mathrm{SM}}$	130.5	71.6	96.1	133.4	192.9	279.3
$\sigma_{\mathrm{ggF+VBF}}/\sigma_{\mathrm{ggF+VBF}}^{\mathrm{SM}}$	$\boxed{5.4}$	4.3	5.8	$\boxed{8.1}$	12.2	19.1

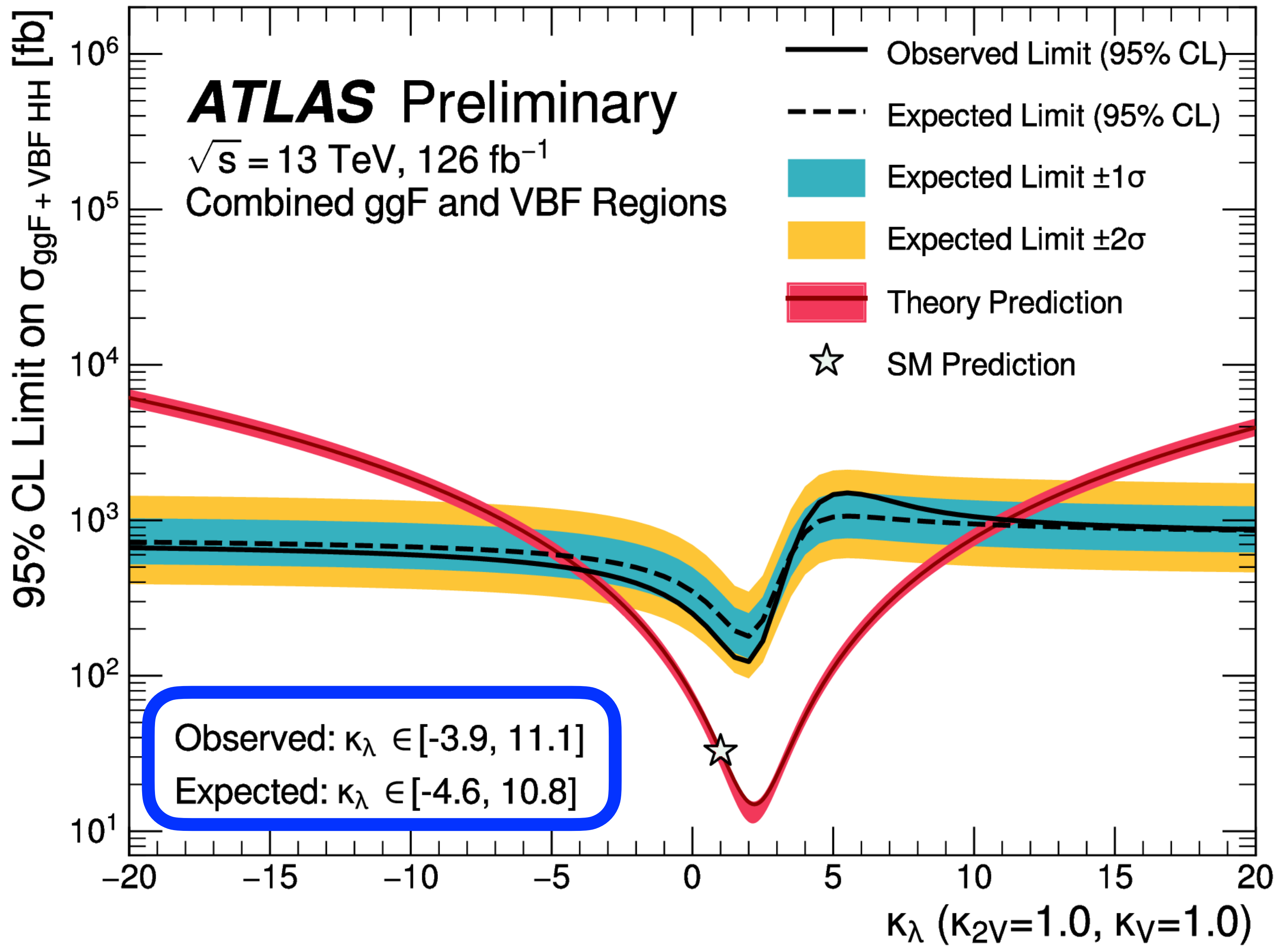

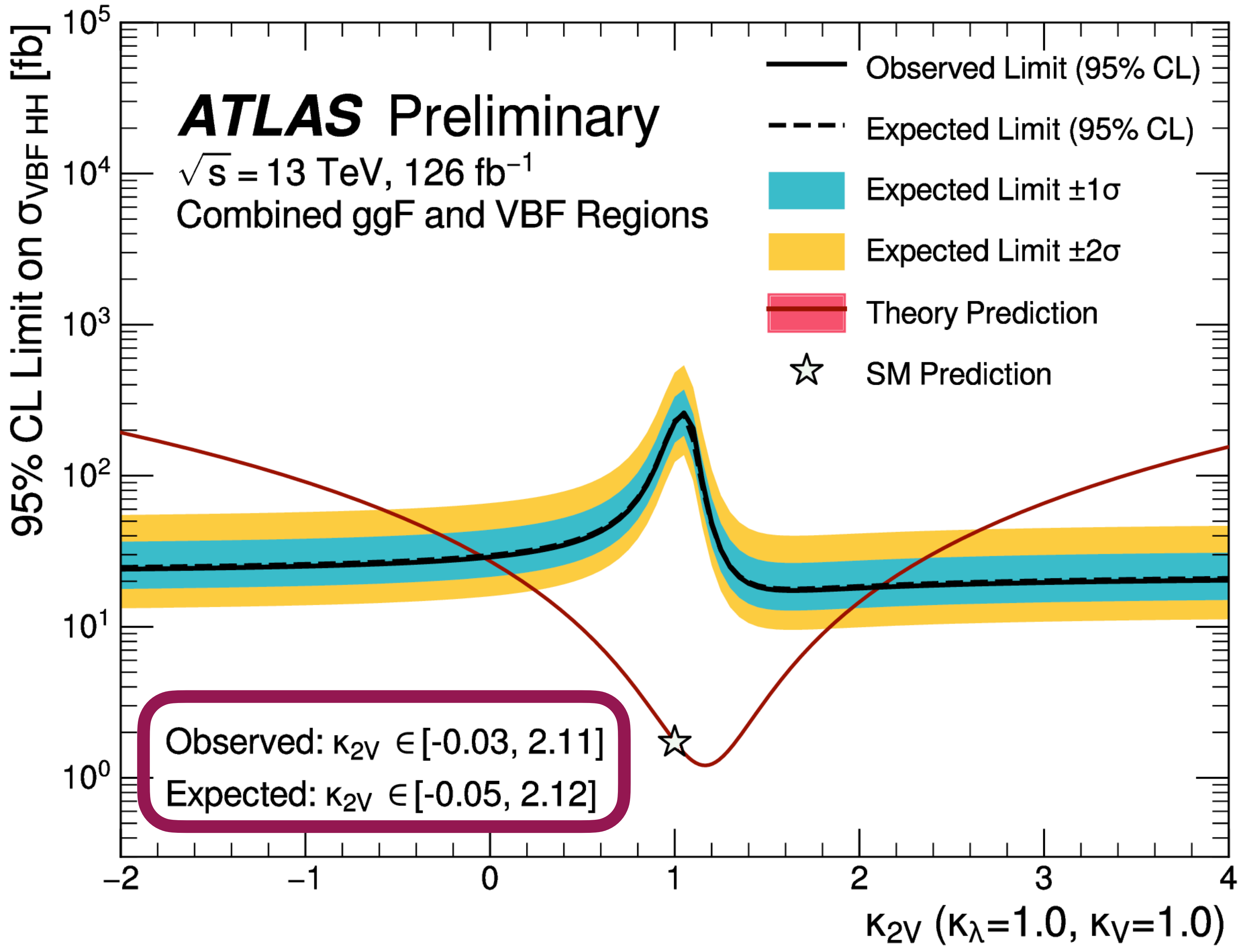

- Factor of 3 improvement is achieved w.r.t to $36fb^{-1}$ HH → bbbb results
- Factor 2 from the luminosity increase rest from improvements in object reconstruction and identification (b-tagging) and event selection and categorisation

Full Run2 data results for non-resonant HH→bbττ

ATLAS-CONF-2021-030

Pros:

- Sizeable branching ratio 7%
- Moderate background contaminations

Cons:

- Neutrinos in τ decays
- Challenging had. τ reconstructions & triggering

- Given the τ decay two sub-channels are considered
  - Semi leptonic $\tau_{Lep}\tau_{Had}$
    - 1 Lepton (e/μ) and 1τ
  - Fully hadronic $\tau_{Had}\,\tau_{Had}$
    - 2 τ

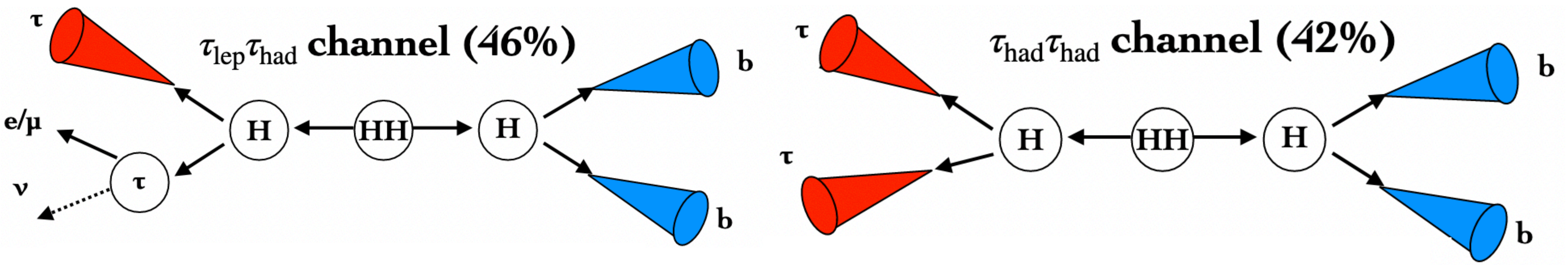

- Triggers:
  - Single-Tau or Di-Tau for $\tau_{Had}\,\tau_{Had}$
  - Single-Lepton (SLT) or Lepton+Tau (LTT) triggers for $\tau_{Lep}\tau_{Had}$

Main backgrounds:

- ttbar and Z+heavy flavour jets (with real τ), modelled with Monte Carlo simulations, with normalisation from fit to data in control regions
- Events with jets faking hadronically decaying τ from ttbar and QCD multi-jet (data-driven fake-factor)

Full Run2 data results for non-resonant HH→bbττ

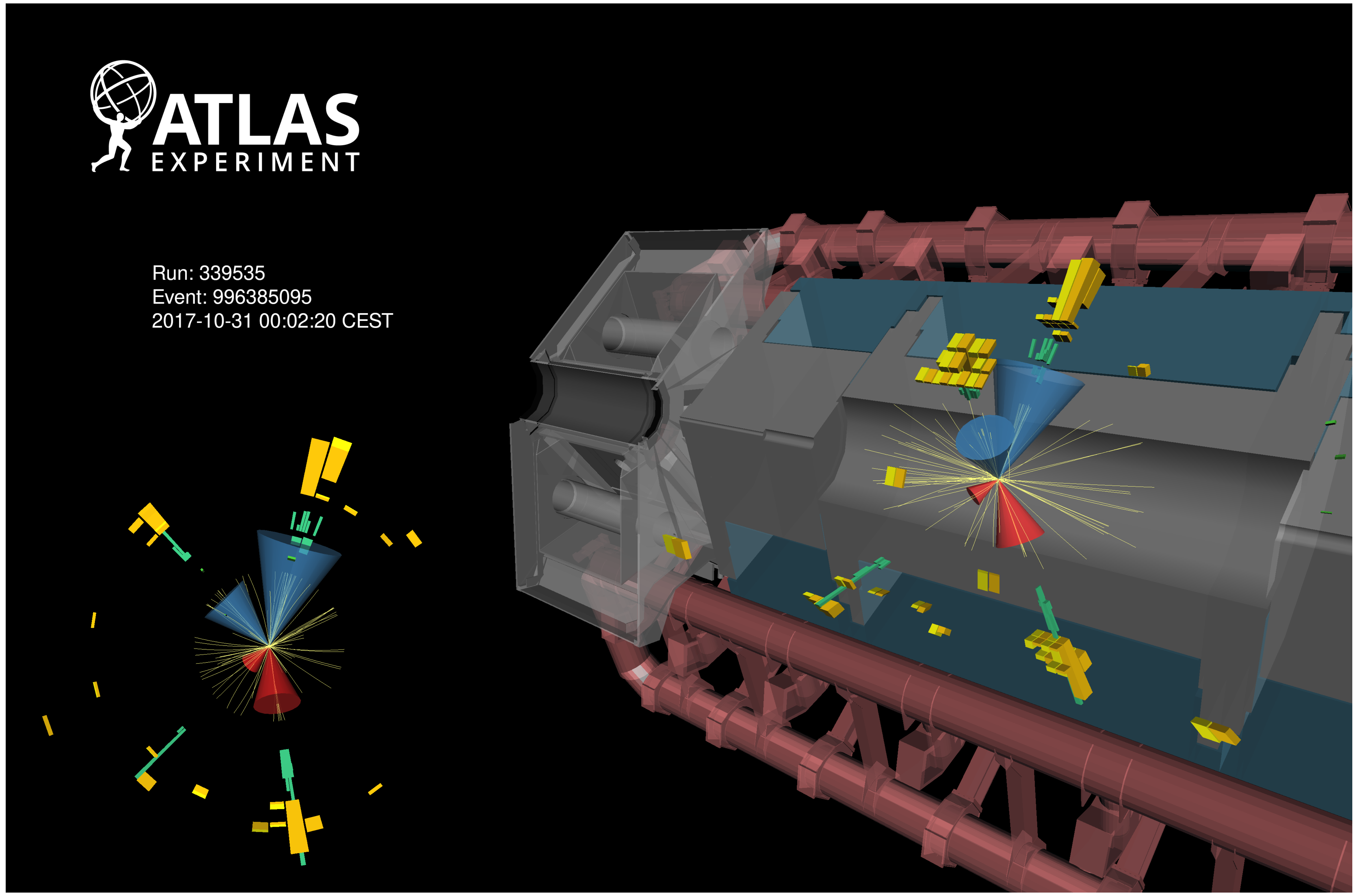

Candidate HH data event in the τ_{lep} τ_{had} channel signal region

$m_{HH} = 680$ GeV, $m_{bb} = 120$ GeV and $m_{\tau\tau} = 120$ GeV

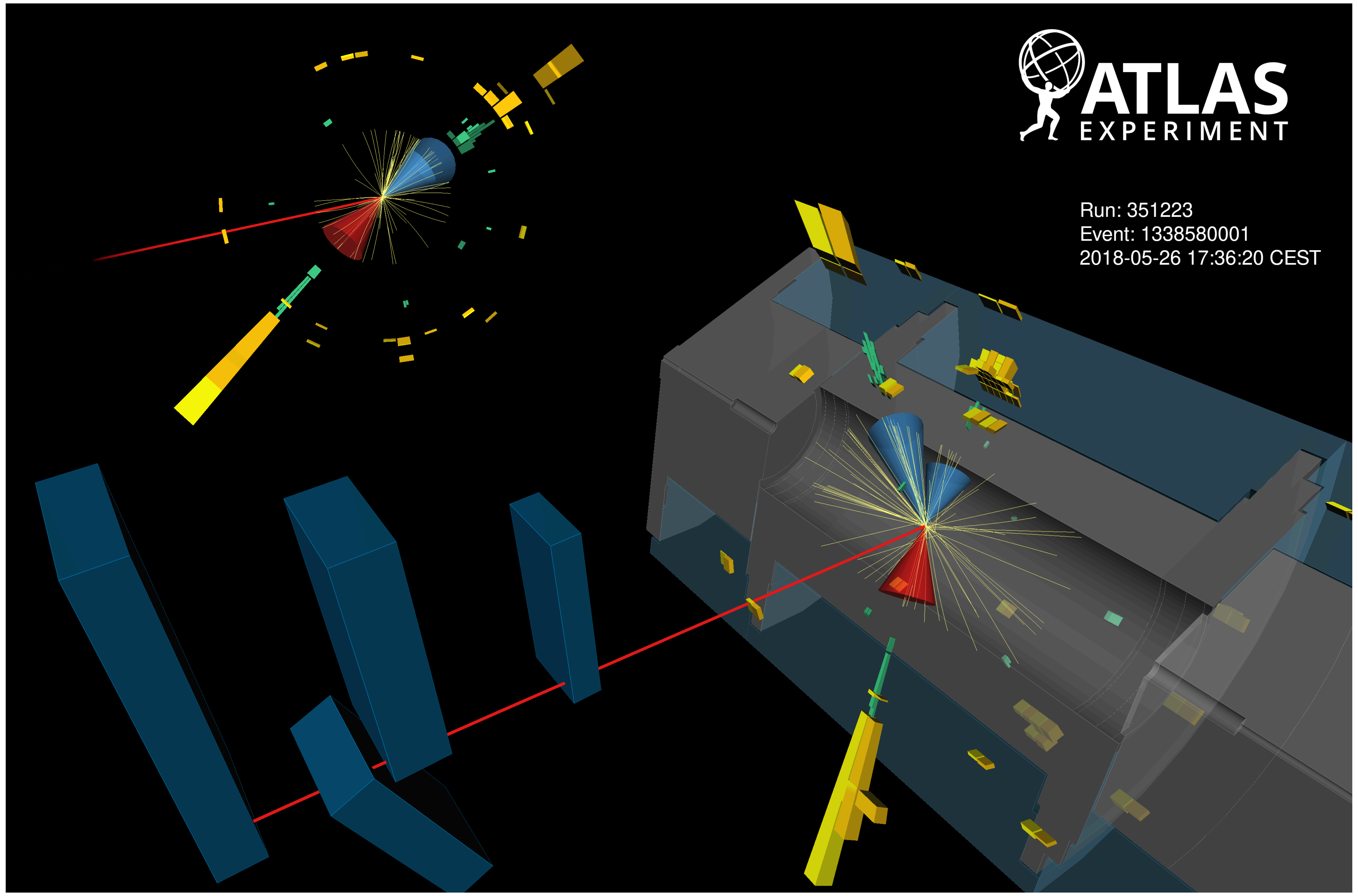

Candidate HH data event in the $\tau_{had}\tau_{had}$ channel signal region

$m_{HH} = 510$ GeV, $m_{bb} = 130$ GeV, and $m_{\tau\tau} = 130$GeV

Full Run2 data results for non-resonant HH→bbττ

- **Signal extractions**
  - Signal/background classifiers provide discriminant for the likelihood fit
    - $\tau_{Had}\ \tau_{Had}$: BDT
    - $\tau_{Lep}\tau_{Had}$: NN
- The most prominent training variables: reconstructed di-Higgs invariant mass m_{HH} , reconstructed invariant masses of the two Higgs boson candidates m_{bb} and $m_{\tau\tau}$

HadHad

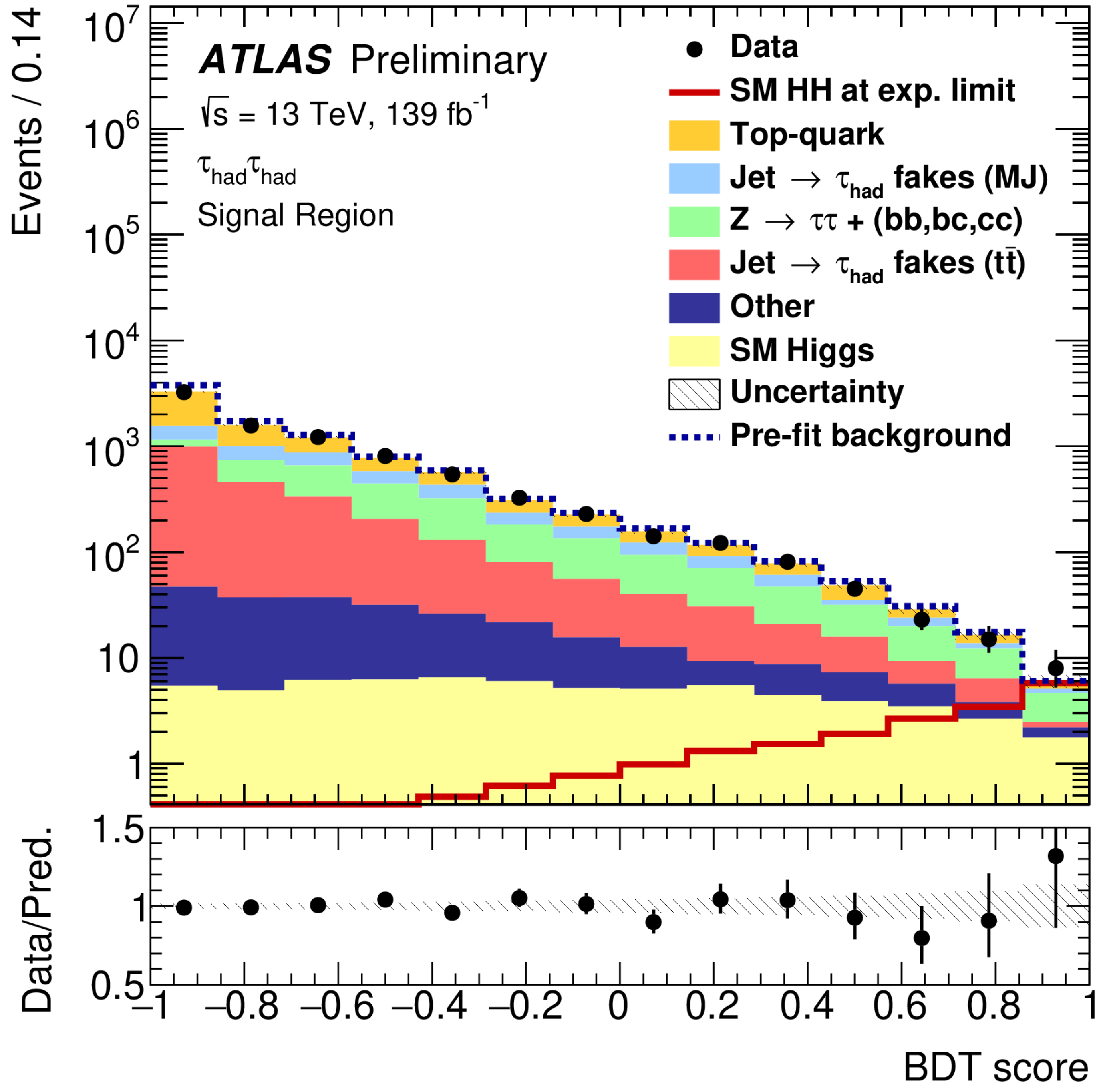

SLT LepHad

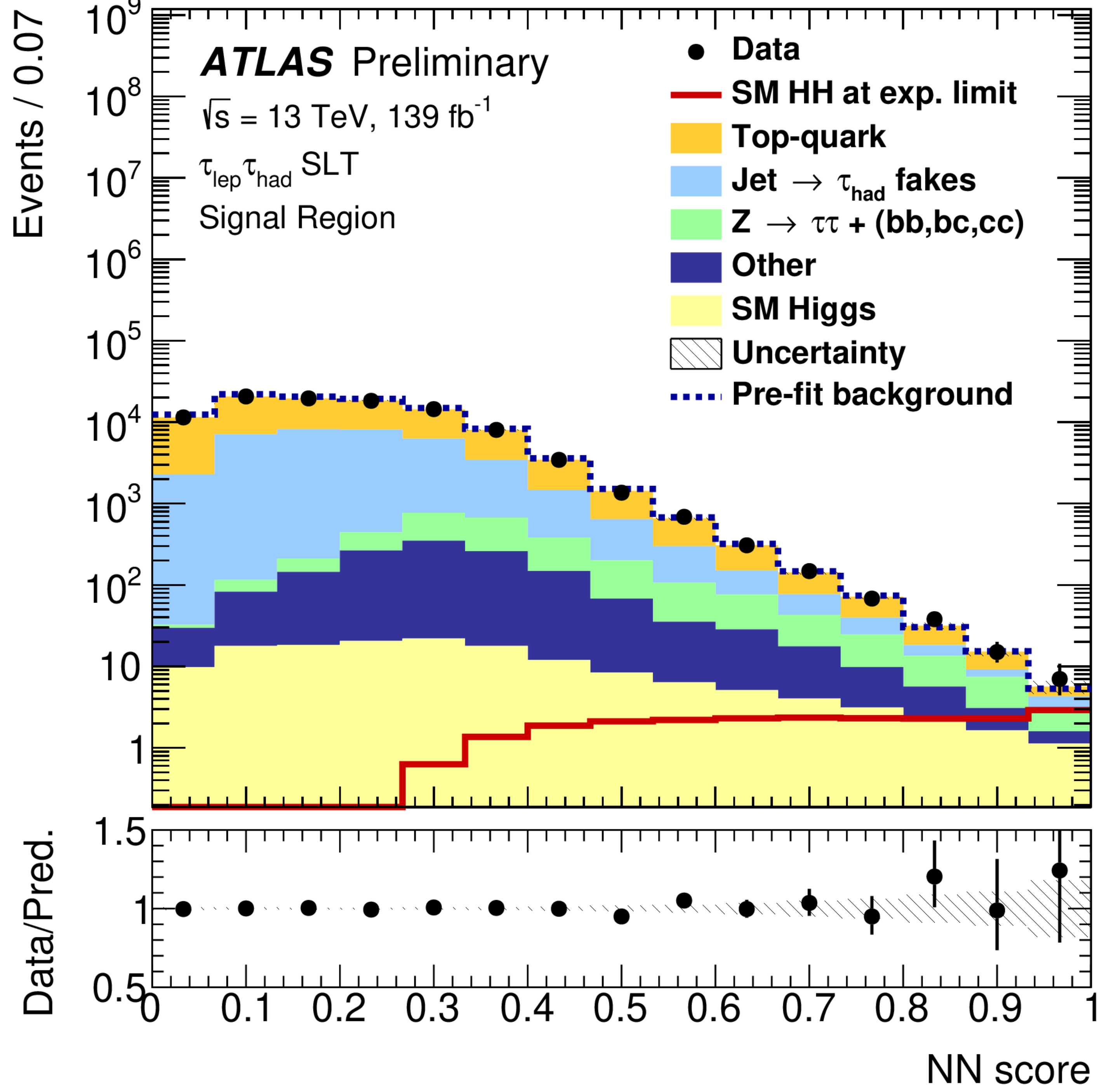

LTT LepHad

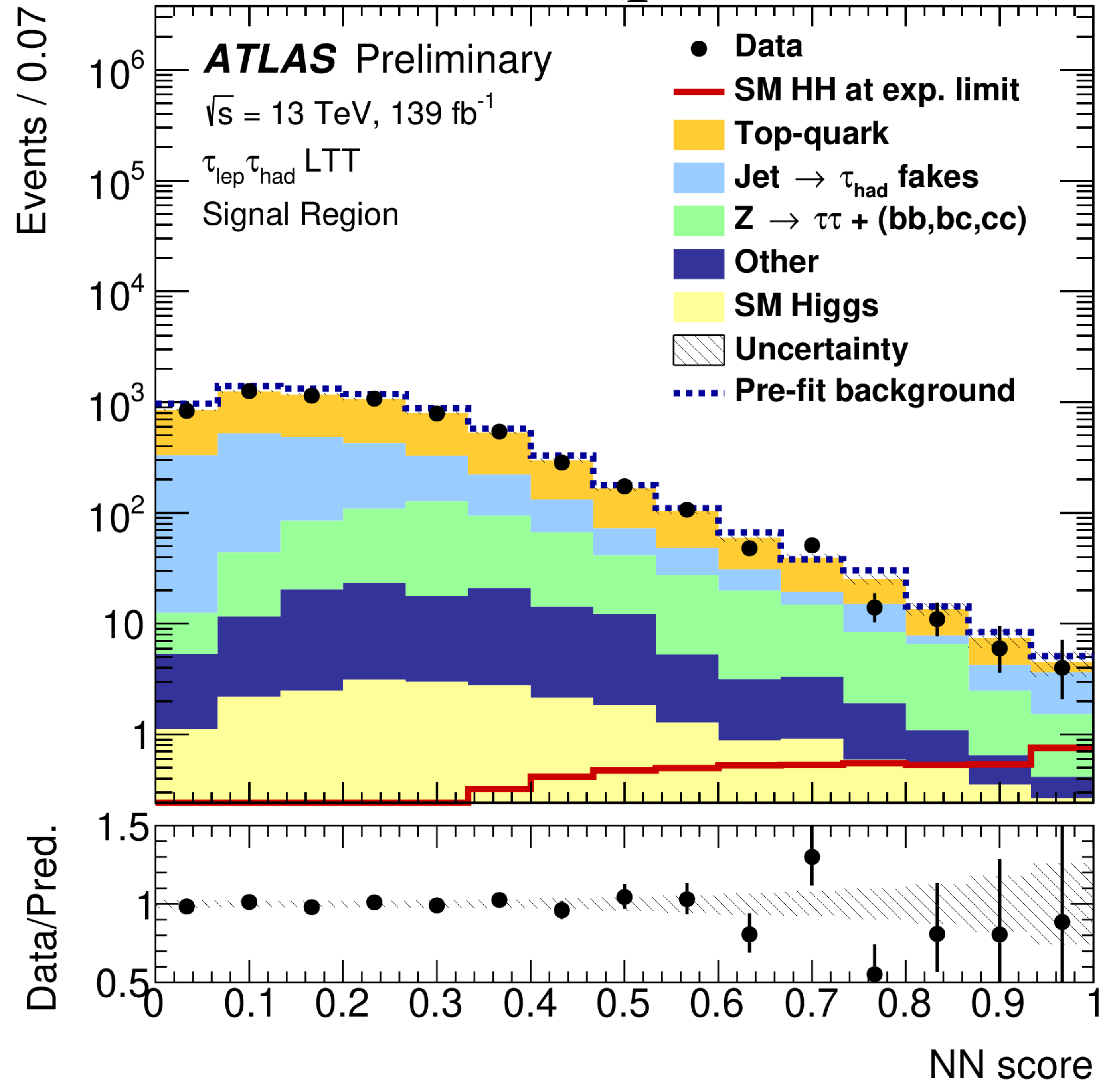

Full Run2 data results for non-resonant HH→bbττ

ATLAS-CONF-2021-030

		Observed	−2 σ	−1 σ	Expected	+1 σ	+2 σ
$\tau_{had}\tau_{had}$	$\sigma_{ggF+VBF}$ [fb]	145	70.5	94.6	131	183	245
	$\sigma_{ggF+VBF}/\sigma^{SM}_{ggF+VBF}$	4.95	2.38	3.19	4.43	6.17	8.27
$\tau_{lep}\tau_{had}$	$\sigma_{ggF+VBF}$ [fb]	265	124	167	231	322	432
	$\sigma_{ggF+VBF}/\sigma^{SM}_{ggF+VBF}$	9.16	4.22	5.66	7.86	10.9	14.7
Combined	$\sigma_{ggF+VBF}$ [fb]	135	61.3	82.3	114	159	213
	$\sigma_{ggF+VBF}/\sigma^{SM}_{ggF+VBF}$	4.65	2.08	2.79	3.87	5.39	7.22

ATLAS-CONF-2021-030

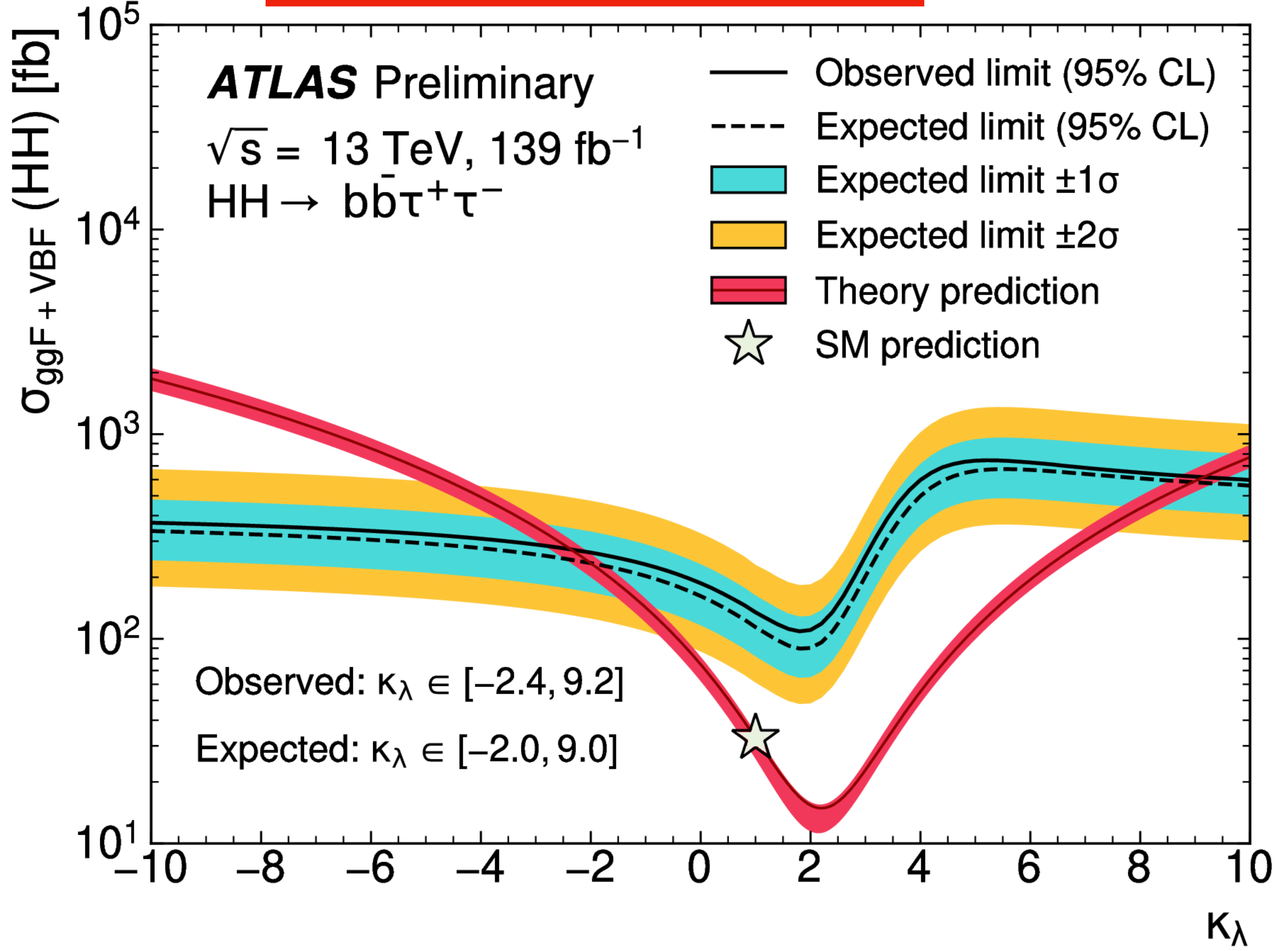

- Factor of 4 improvement is achieved w.r.t to $36fb^{-1}$ HH → bbττ results
- The factor 2 from luminosity increase and factor 2 from improvements in objects reconstruction and event selection b-tagging and τ-identification

Full Run2 data results for non-resonant HH→bbγγ

arXiv:2112.11876

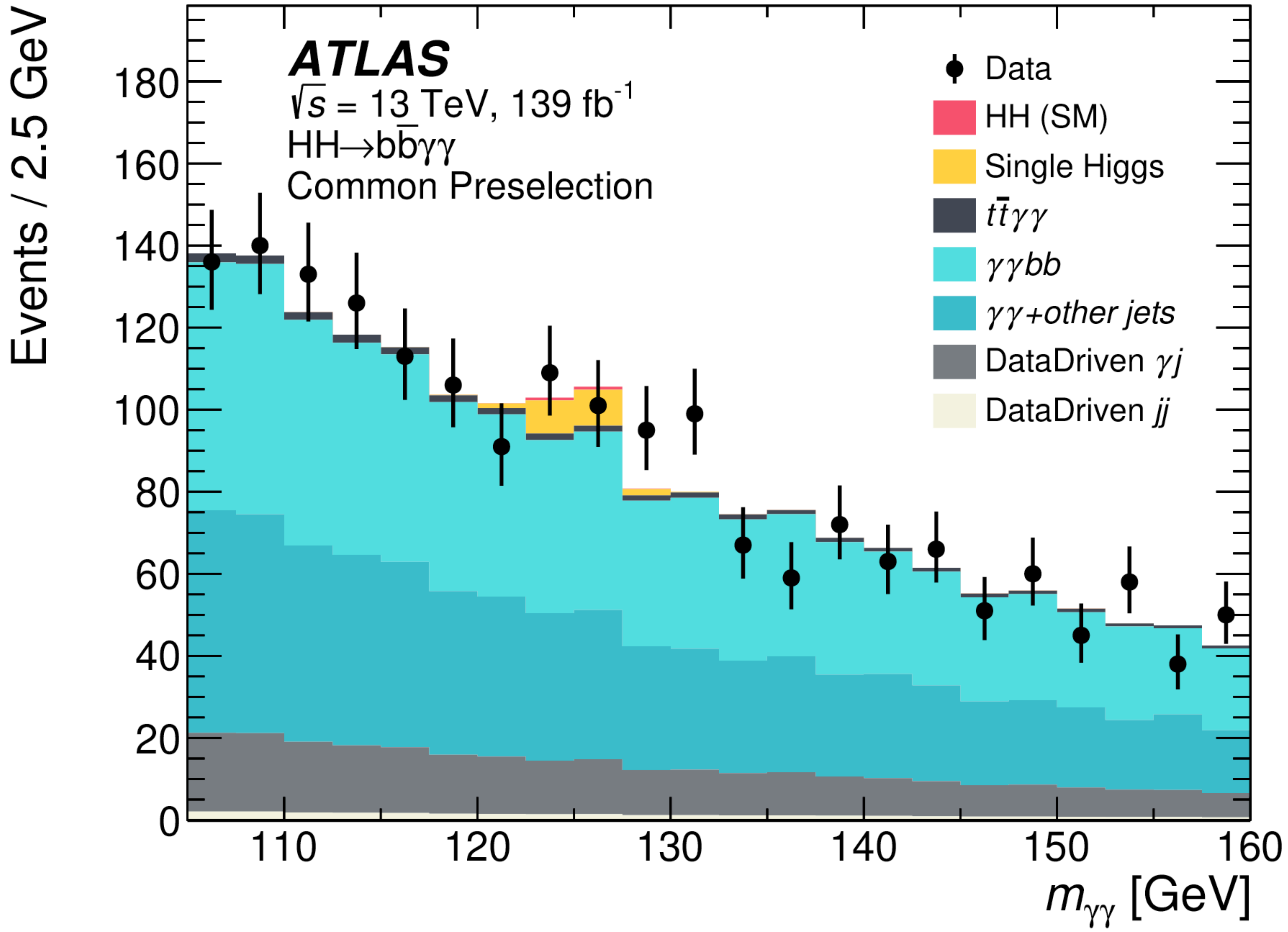

- Search for SM and BSM non-resonant HH production
- HH→bbγγ has the lower BR(0.26%) but this offering a very clean photons signatures and clean smoothly falling di-photon background
- 2b-tagged jets and two photons
- 105 GeV < $m_{\gamma\gamma}$ < 160 GeV

- **Major backgrounds:** γγ+jets modelled with exponential function derived from data in CRs and single-Higgs modelled with double-sided Crystal-Ball function derived from Monte Carlo simulations
- **Boosted Decision Trees** used to discriminate signal and background
- **Important input variable:** reconstructed invariant mass of the Higgs boson candidate m_{bb}

Full Run2 data results for non-resonant HH→bbγγ

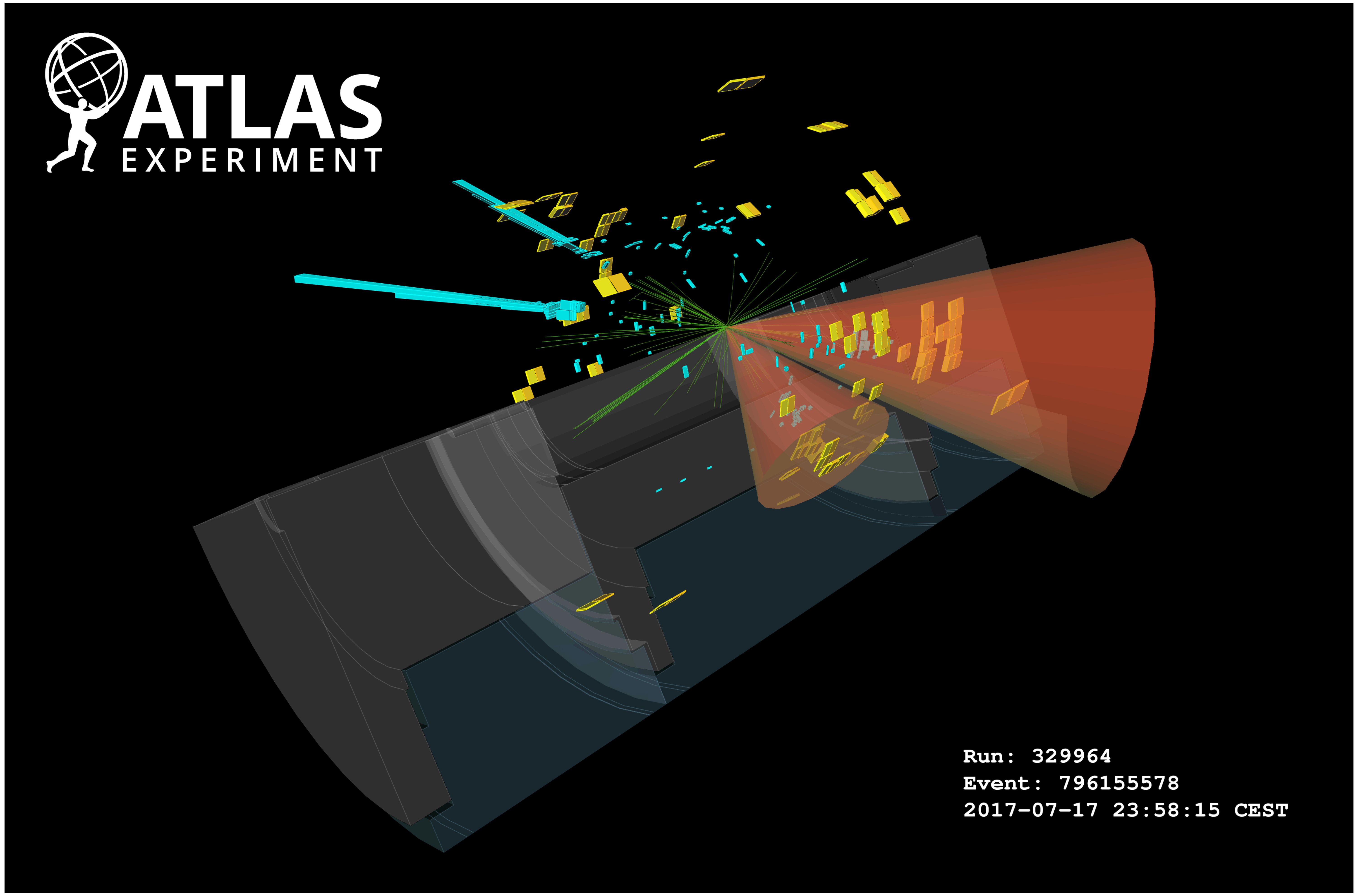

Candidate HH data event of the non-resonant high mass BDT tight signal region

m_{HH} = 625 GeV, m_{bb} = 113 GeV and $m_{\gamma\gamma}$ = 123 GeV

Full Run2 data results for non-resonant HH→bbγγ

arXiv:2112.11876

The $m_{\gamma\gamma}$ is used as final discriminant variable in the 4 regions

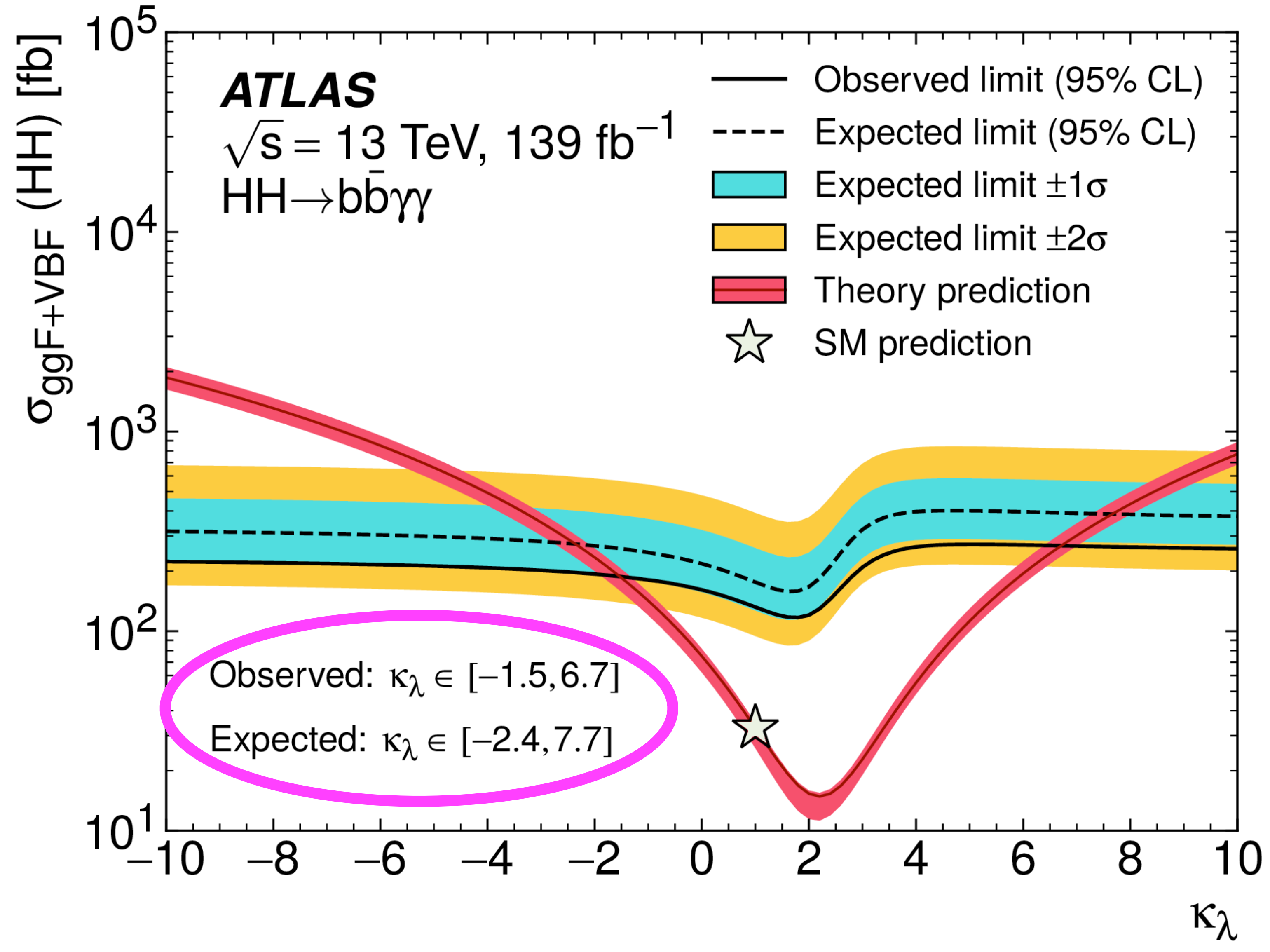

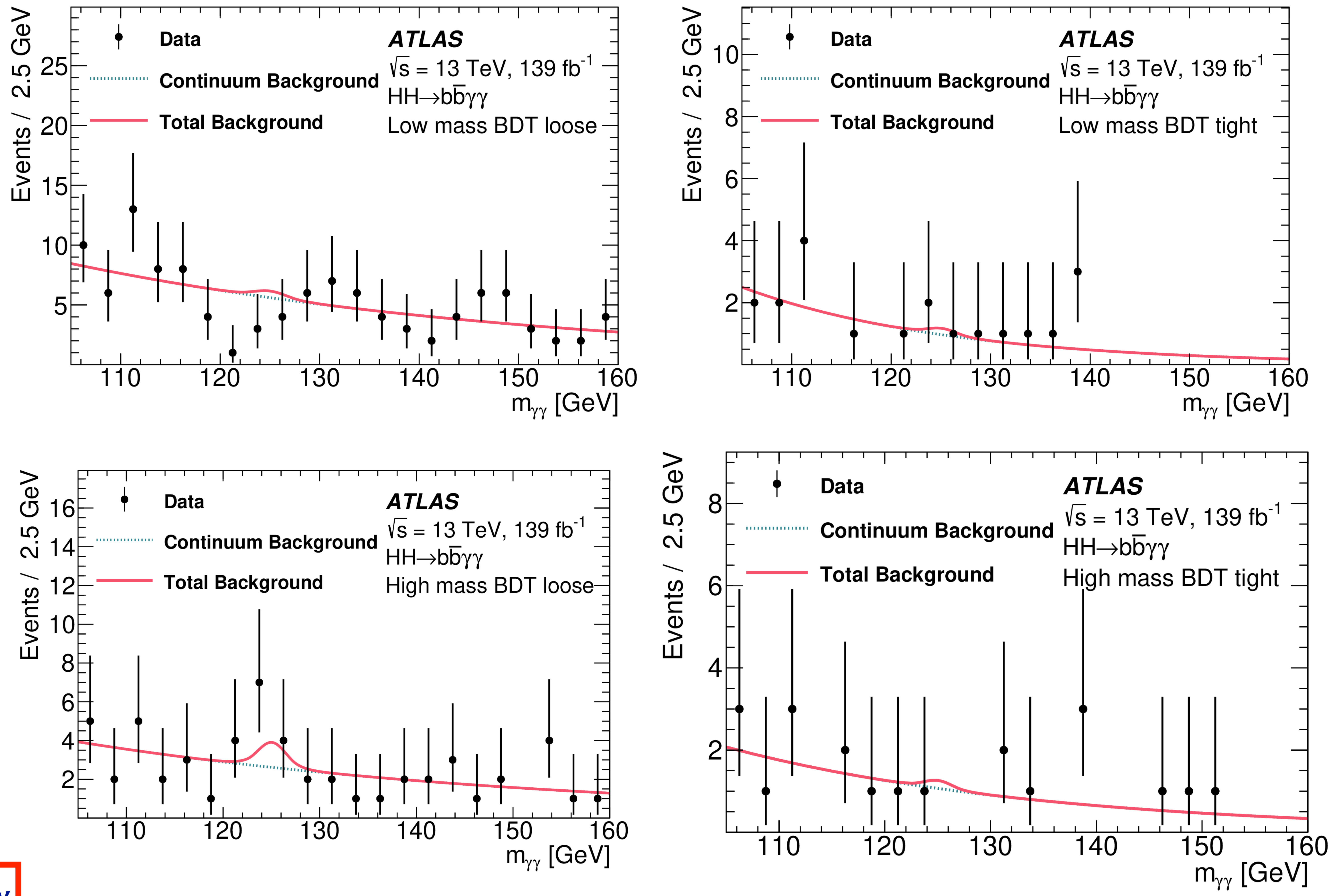

Factor of 5 improvement compared to $36fb^{-1}$ bbγγ results: factor 2 from luminosity increase and factor 3 from improvements in objects reconstruction and identification (b-tagging) and event categorisation in

Upper limit on the non-resonant ggF+VBF HH cross section of 4.2 x SM observed (5.7 x SM expected)

Full Run2 data results for non-resonant HH combination

- The combination of HH is performed in bbbb, bbττ, bbγγ decay channel using full LHC Run2 data of $139 fb^{-1}$:

- observed (expected) upper limit of 2.4 (2.9) at 95% CL has been set on the HH signal strength defined as the sum of the ggF HH and VBF HH production cross-section normalised to its SM prediction

ATLAS-CONF-2022-050

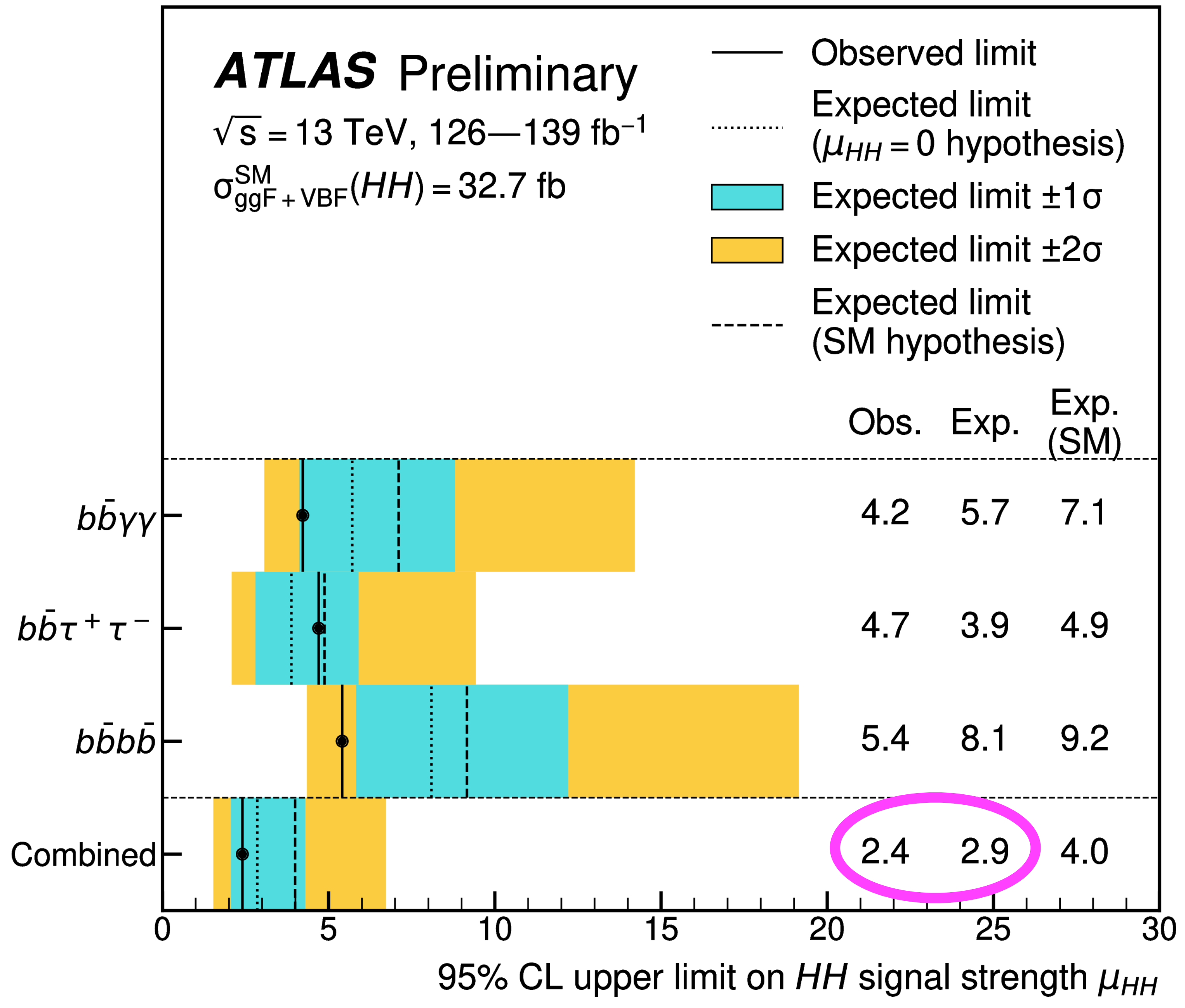

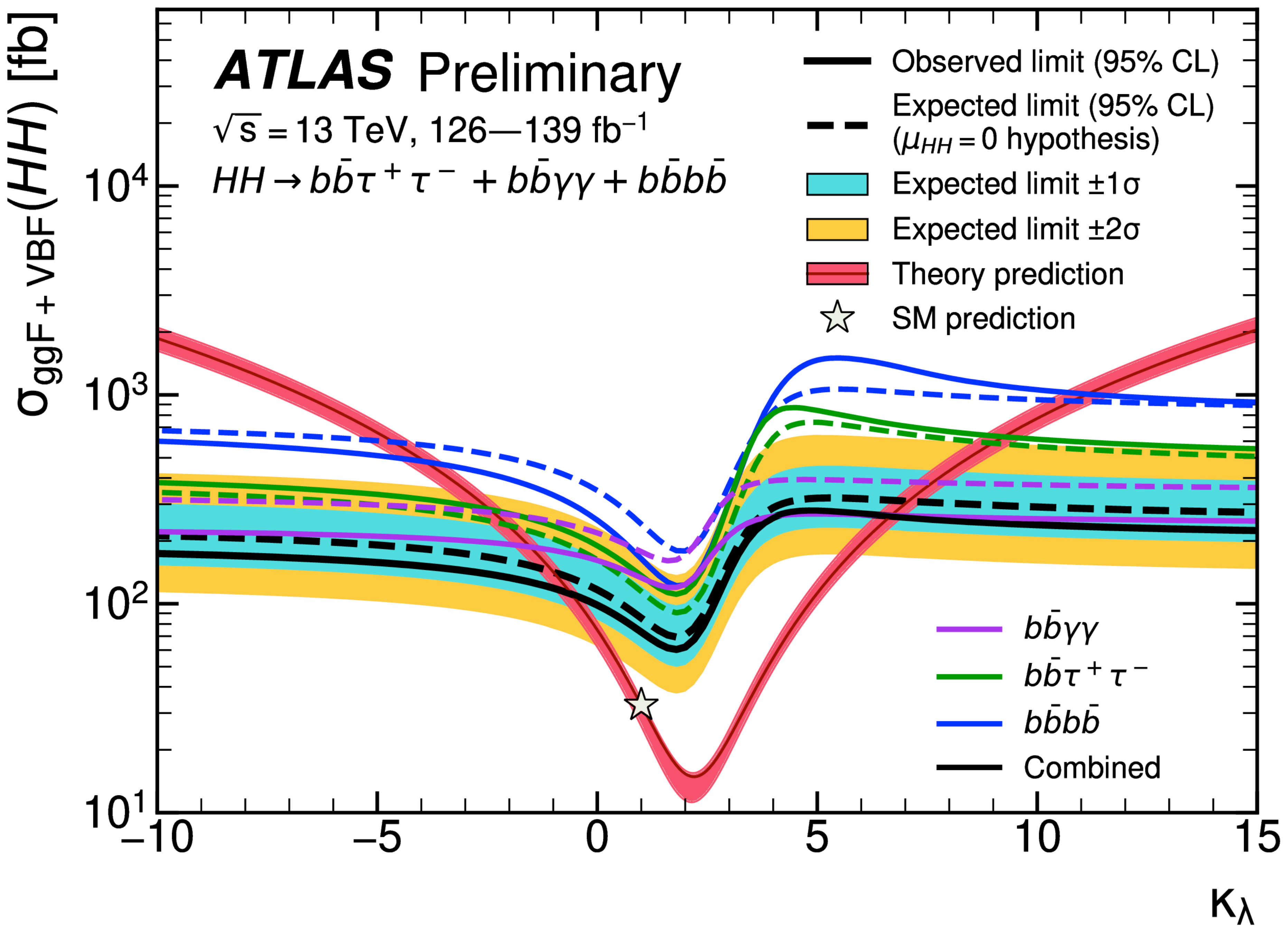

Improvement of more than a factor 3 compared to $36 fb^{-1}$ dataset combination (even including less decay channels) World's best upper limit on non-resonant HH production and constraints on κ_λ up to now

Prospects High Luminosity LHC (HL-LHC)

Extrapolations of new ATLAS full run2 non-resonant HH searches in the $bb\tau\tau$ and $bb\gamma\gamma$ channels to HL-LHC with 3000 fb^{-1}

ATL-PHYS-PUB-2022-005

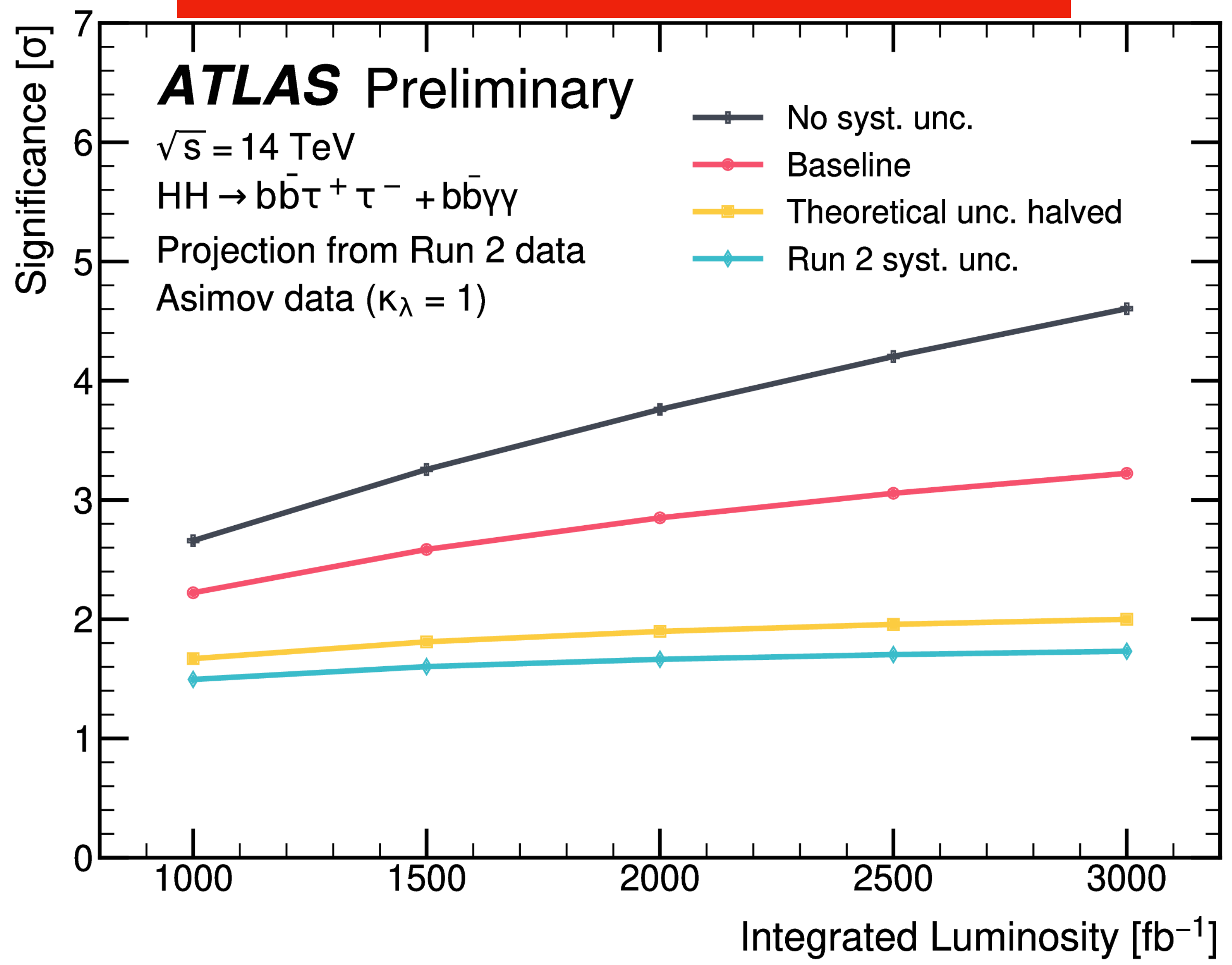

Uncertainty scenario	Significance [σ] $b\bar{b}\gamma\gamma$	$b\bar{b}\tau^+\tau^-$	Combination	Combined signal strength precision [%]
No syst. unc.	2.3	4.0	4.6	$-23/+23$
Baseline	2.2	2.8	3.2	$-31/+34$
Theoretical unc. halved	1.1	1.7	2.0	$-49/+51$
Run 2 syst. unc.	1.1	1.5	1.7	$-57/+68$

Baseline:
The systematic uncertainties are adjusted following the latest recommendations from HL-LHC [Link]

ATL-PHYS-PUB-2022-005

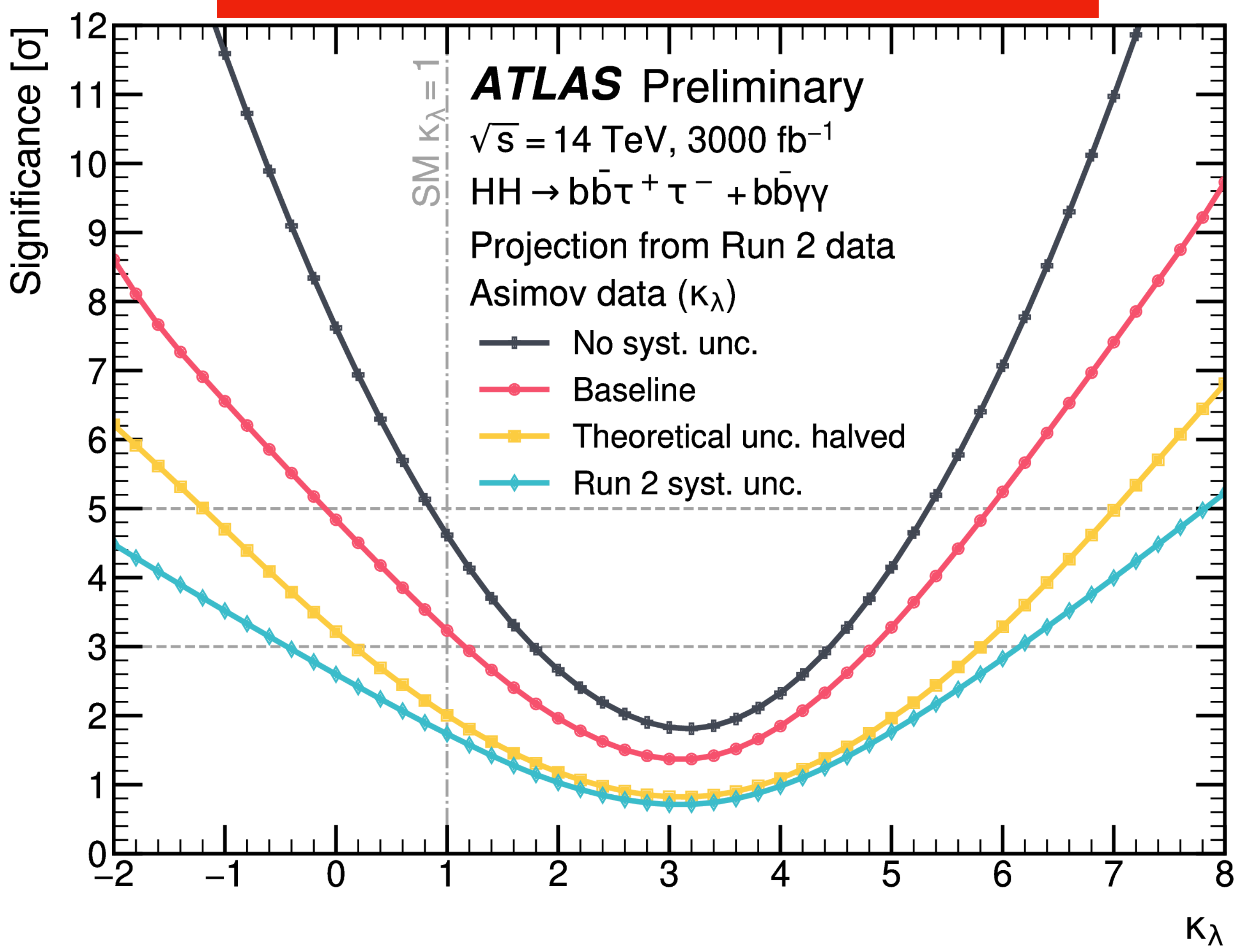

Uncertainty scenario	Likelihood scan 1 σ CI	Likelihood scan 2 σ CI
No syst. unc.	$[0.6, 1.5]$	$[0.3, 2.1]$
Baseline	$[0.5, 1.6]$	$[0.0, 2.7]$
Theoretical unc. halved	$[0.2, 2.2]$	$[-0.4, 5.6]$
Run 2 syst. unc.	$[0.1, 2.5]$	$[-0.7, 5.7]$

Baseline scenario: Expected significance of 3.2σ and 30% uncertainty on the signal strength for SM HH signal
Systematic uncertainties will become important at the HL-LHC

Baseline scenario: 50% uncertainty on κ_λ for SM Higgs
New projected precision from ATLAS alone is of the same order of the previous ATLAS+CMS projection!

Summary of searches for resonant HH production

Resonant HH combination with full Run 2 data

- Searches are performed for BSM resonant HH production: resonance mass point ∈ [0.25, 5] TeV
- $X \rightarrow HH \rightarrow bbbb$, $bb\tau\tau$, $bb\gamma\gamma$
- Similar baseline event selections and background estimations to the non-resonant searches in the same final states
- Optimised signal region selections and discriminants specifically for the resonant signals

ATLAS-CONF-2021-052

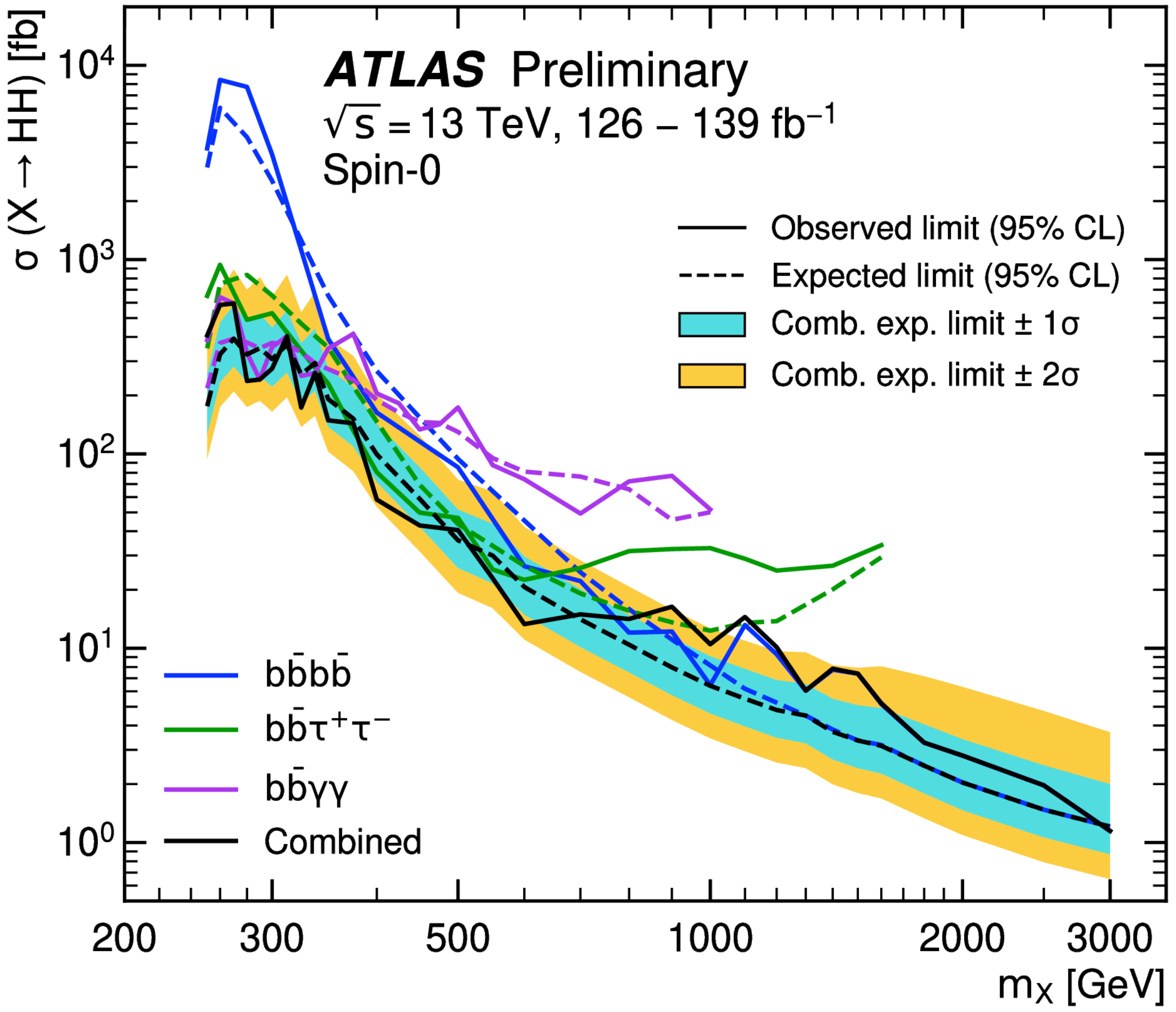

Small data excess at 1.1 TeV, significance of 3.2σ (2.1σ) local (global)

Combination of HH analyses performed in 3 decay channels using full LHC Run 2 data corresponding to :

- $bb\tau\tau$, $bb\gamma\gamma$ and bbbb channels for the searches for resonant HH production 139 fb^{-1}

Complementarity of searches in different decay channels:

$bb\gamma\gamma$ best sensitivity at low mass **ATLAS-CONF-2021-030**

$bb\tau\tau$ best sensitivity in medium mass range **arXiv:2112.11876**

bbbb best sensitivity at high mass **Phys. Rev. D 105 092002**

Summary and conclusion

- HH searches allows to probe directly the Higgs self coupling
- ATLAS analysis on HH for the decay channels bbbb, bbττ and bbγγ have attained significant improvement in comparison to the previous result performed on 36 fb^{-1} data
- In combination of the HH decay channels ATLAS has achieved most stringent limits on non-resonant HH production and most stringent constraints on κ_λ until now

The Observed upper limit 2.4 at 95 % CL
$-0.6 < \kappa_\lambda < 6.6$ at 95% CL

- New HL-LHC extrapolations based on latest results improved compared to the ones based on the 36 fb^{-1} analyses:
    - Expected more than 3.0 σ evidence and 50 % uncertainty on κ_λ for SM HH from ATLAS

Thanks for listening

Back-up Slides

ggF HH pair production

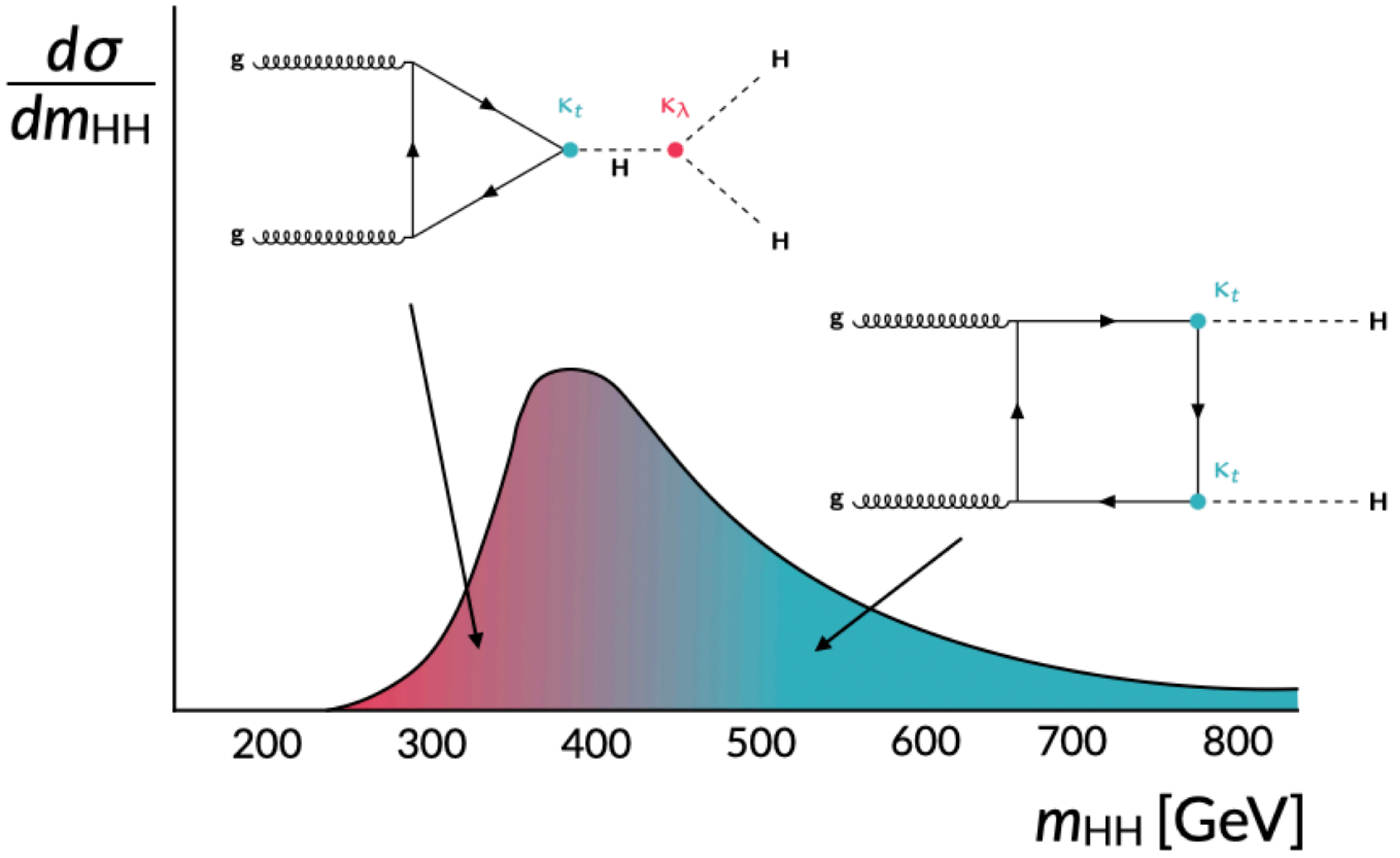

Full run2 data results for $HH \to bbbb$

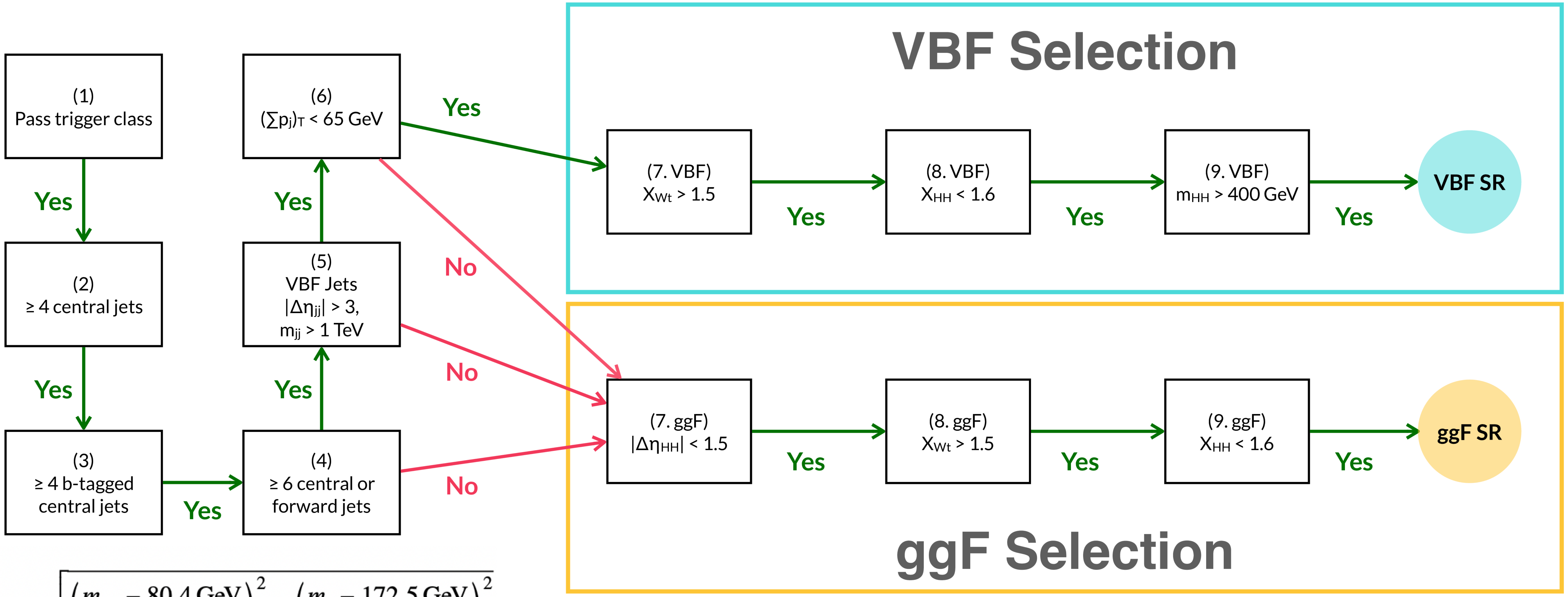

$$X_{Wt} = \sqrt{\left(\frac{m_W - 80.4\,\mathrm{GeV}}{0.1\,m_W}\right)^2 + \left(\frac{m_t - 172.5\,\mathrm{GeV}}{0.1\,m_t}\right)^2}$$

A flowchart summarizing the analysis selection. Events must pass selection criteria 1-3 in order to be considered for either analysis signal region. Events failing any of the selection criteria 4-6 are considered for inclusion in the ggF signal region, while those passing selection criteria 4-6 are considered for the VBF signal region. The X_{Wt} variable in the figure denotes the minimum value of the X_{Wt} variable as obtained from the different combinations of central and b-tagged jets in the event.

Full run2 data results for $HH \to bbbb$

Category	Data	Expected Background	ggF Signal SM	VBF Signal SM
ggF signal region				
$\|\Delta\eta_{HH}\| < 0.5,\ X_{HH} < 0.95$	1940	1940(130)	6.99	0.038
$\|\Delta\eta_{HH}\| < 0.5,\ X_{HH} > 0.95$	3602	3620(200)	6.49	0.036
$0.5 < \|\Delta\eta_{HH}\| < 1.0,\ X_{HH} < 0.95$	1924	1870(120)	5.15	0.037
$0.5 < \|\Delta\eta_{HH}\| < 1.0,\ X_{HH} > 0.95$	3540	3490(190)	4.75	0.040
$\|\Delta\eta_{HH}\| > 1.0,\ X_{HH} < 0.95$	1880	1740(120)	2.92	0.043
$\|\Delta\eta_{HH}\| > 1.0,\ X_{HH} > 0.95$	3285	3210(200)	2.81	0.041
VBF signal region				
$\|\Delta\eta_{HH}\| < 1.5$	116	125(12)	0.37	0.090
$\|\Delta\eta_{HH}\| > 1.5$	241	231(20)	0.06	0.207

The yields in each analysis category of the data, expected background, and expected SM ggF and VBF signals. The expected background yields are obtained using a background-only fit to the data. The expected signal yields are obtained from simulation.

Full run2 data results for $HH \to bbbb$

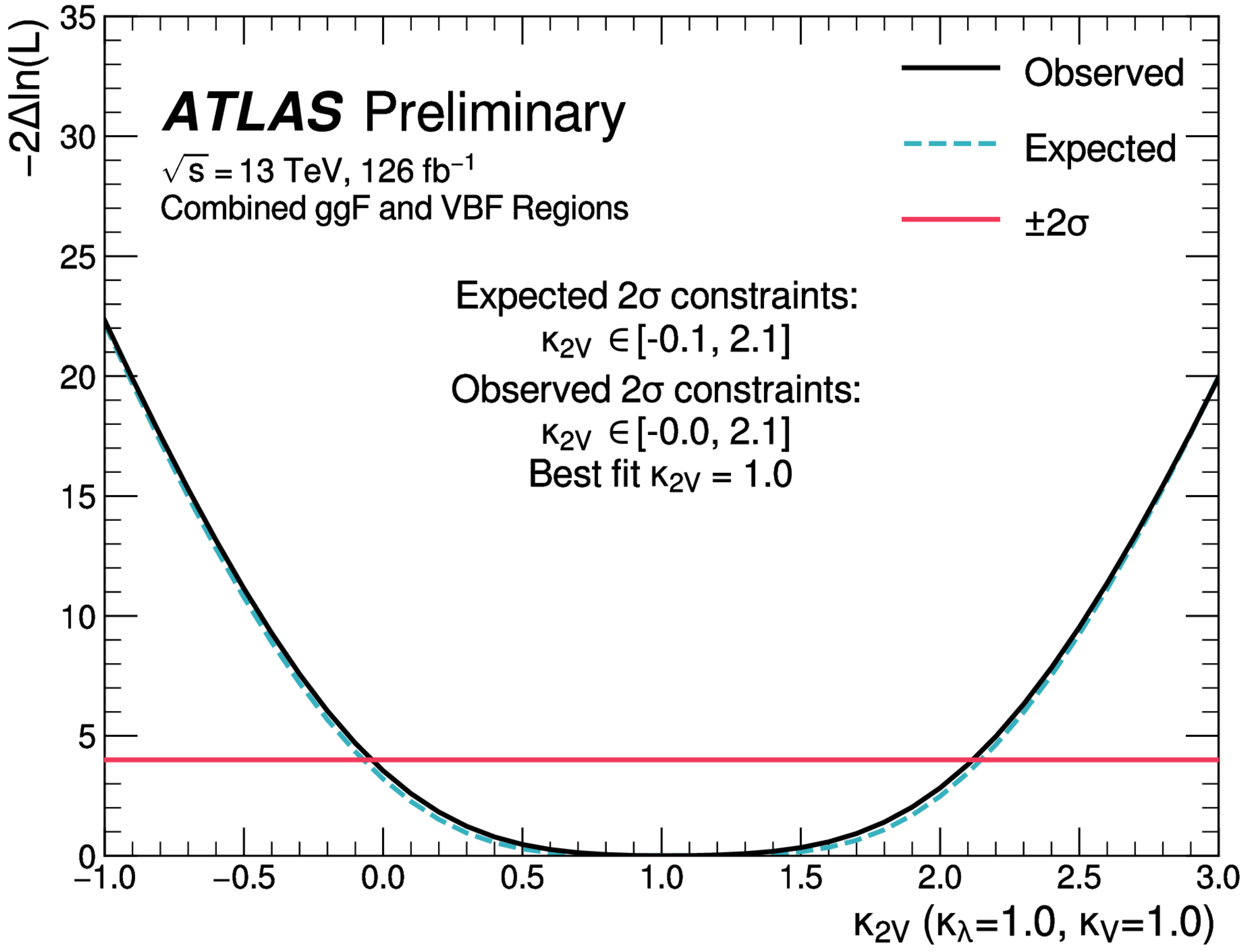

The observed profile likelihood ratio scans for the (a) κ_λ and (b) κ_{2V} coupling modifiers, shown by the solid black line, using the coupling modifiers **κ** as the POIs. The values of the other two parameters (κ_V and κ_{2V} in (a) and κ_V and κ_λ in (b)) are fixed to 1. The dashed blue line shows the expected exclusion limits, as obtained using a background-only fit to the data. The pink line indicates the 2σ exclusion boundary.

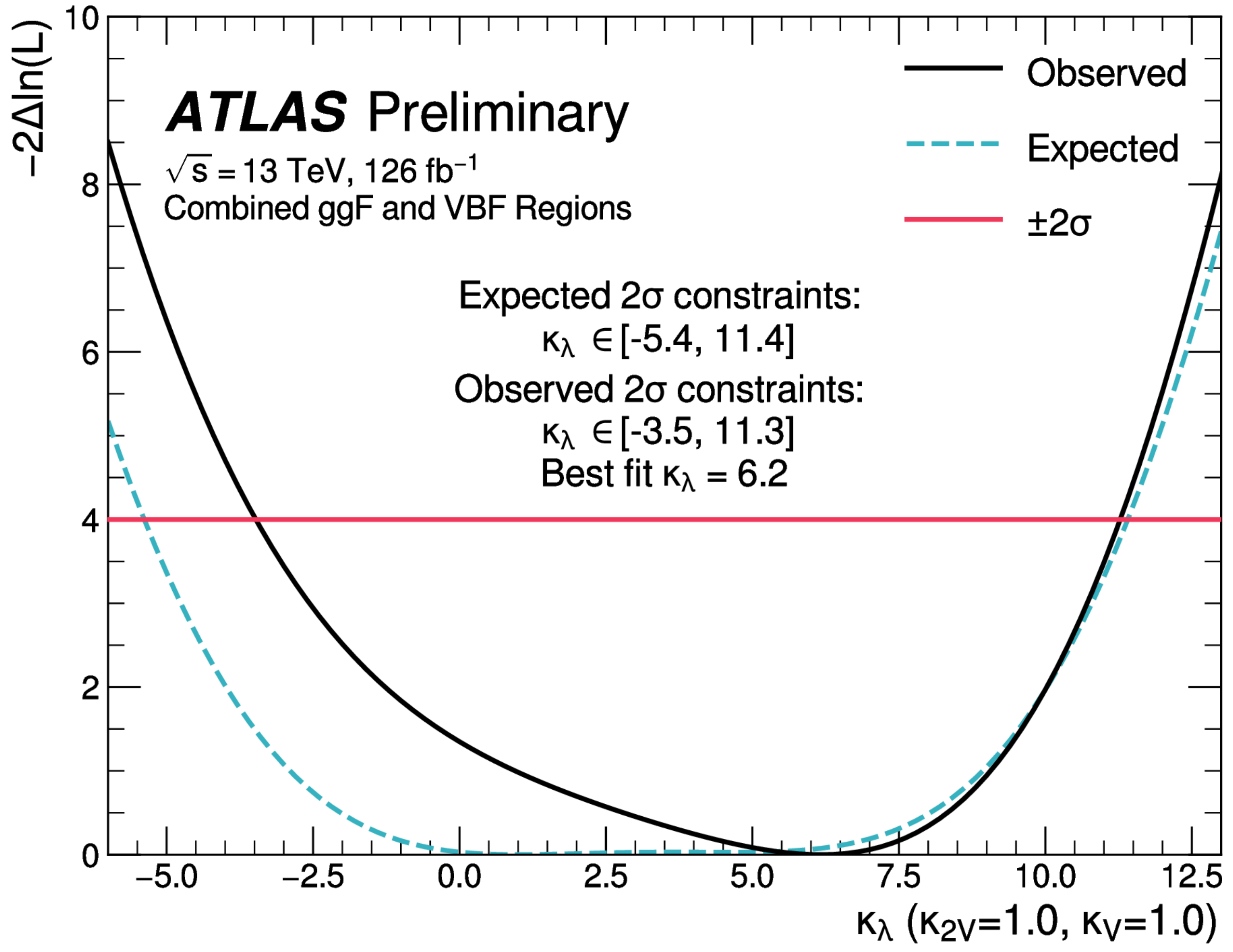

The observed profile likelihood ratio scans for the (a) κ_λ and (b) κ_{2V} coupling modifiers, shown by the solid black line, using the coupling modifiers **κ** as the POIs. The values of the other two parameters (κ_V and κ_{2V} in (a) and κ_V and κ_λ in (b)) are fixed to 1. The dashed blue line shows the expected exclusion limits, as obtained using a background-only fit to the data. The pink line indicates the 2σ exclusion boundary.

Full run2 data results for $HH \to bbbb$

The background estimation makes use of an alternative set of events, which pass the same b-jet triggers and satisfy all the same selection criteria as the $4b$ events, with one difference: they are required to contain exactly two b-tagged jets. This sample, referred to hereafter as "$2b$", has about two orders of magnitude more events than the $4b$ sample, hence the presence in it of any $HH \to b\bar{b}b\bar{b}$ signal is negligible, making it suitable for the background estimation. The jets selected to form the two Higgs boson candidates in the $2b$ events are the two b-tagged jets and the two untagged jets with the highest p_{T} (excluding the VBF jets in the VBF categories).

The kinematic properties of the $2b$ and $4b$ events are not expected to be identical, partly due to different processes contributing to the two samples, but also due to differences in the trigger acceptance and because the performance of b-tagging varies as a function of jet p_{T} and η. Therefore, a reweighting function is required, which, when applied to the $2b$ events, maps their kinematic distributions onto the corresponding $4b$ distributions. This function is derived using the $2b$ and $4b$ events in a *control region* (CR) surrounding the SR in the reconstructed (m_{H1}, m_{H2}) plane and then applied to the $2b$ events in the SR to produce the background estimate. The "inner edge" of the CR is defined by $X_{HH} = 1.6$ and the "outer edge" by:

$$\sqrt{\left(m_{H1} - 1.05 \cdot 124\,\mathrm{GeV}\right)^2 + \left(m_{H2} - 1.05 \cdot 117\,\mathrm{GeV}\right)^2} = 45\,\mathrm{GeV}\,.$$

Background Estimations using data driven method in 4b

Full run2 data results for non-resonant HH→bbττ

HH bbττ: Event Selection

$\tau_{had}\tau_{had}$ category		$\tau_{lep}\tau_{had}$ categories	
single-τ trigger STT	di-τ trigger DTT	single-lepton trigger SLT	lepton-τ trigger LTT
e/μ selection			
No loose e/μ with $p_T > 7$ GeV		Exactly one tight e or medium μ	
		$p_T^e > 25, 27$ GeV	$18 \text{ GeV} < p_T^e <$ SLT cut
		$p_T^\mu > 21, 27$ GeV	$15 \text{ GeV} < p_T^\mu <$ SLT cut
		$\lvert\eta^e\rvert < 2.47$, not $1.37 < \lvert\eta^e\rvert < 1.52$	
		$\lvert\eta^\mu\rvert < 2.7$	
$\tau_{\text{had-vis}}$ selection			
Two loose $\tau_{\text{had-vis}}$		One loose $\tau_{\text{had-vis}}$	
$\lvert\eta\rvert < 2.5$		$\lvert\eta\rvert < 2.3$	
$p_T > 100, 140, 180$ (25) GeV	$p_T > 40$ (30) GeV	$p_T > 20$ GeV	$p_T > 30$ GeV
Jet selection			
≥ 2 jets with $\lvert\eta\rvert < 2.5$			
$p_T > 45$ (20) GeV	Trigger dependent	$p_T > 45$ (20) GeV	Trigger dependent
Event-level selection			
Trigger requirements passed			
Collision vertex reconstructed			
$m_{\tau\tau}^{\text{MMC}} > 60$ GeV			
Opposite-sign electric charges of $e/\mu/\tau_{\text{had-vis}}$ and $\tau_{\text{had-vis}}$			
Exactly two b-tagged jets			
		$m_{bb} < 150$ GeV	

Full run2 data results for non-resonant HH→bbττ

Process	ME generator	ME PDF	PS and hadronisation	UE model tune	Cross-section order ace2.5cm
Signal					
non-resonant $gg \to HH$ (ggF)	Powheg-Box v2	PDF4LHC15 NLO	Pythia 8.244	A14	NNLO FTApprox
non-resonant $qq \to qqHH$ (VBF)	MadGraph5_aMC@NLO v2.7.3	NNPDF3.0NLO	Pythia 8.244	A14	N3LO(QCD)
resonant $gg \to X \to HH$	MadGraph5_aMC@NLO v2.6.1	NNPDF2.3LO	Herwig v7.1.3	H7.1-Default	–
Top-quark					
$t\bar{t}$	Powheg-Box v2	NNPDF3.0NLO	Pythia 8.230	A14	NNLO+NNLL
t-channel	Powheg-Box v2	NNPDF3.0NLO	Pythia 8.230	A14	NLO
s-channel	Powheg-Box v2	NNPDF3.0NLO	Pythia 8.230	A14	NLO
Wt	Powheg-Box v2	NNPDF3.0NLO	Pythia 8.230	A14	NLO
$t\bar{t}Z$	Sherpa 2.2.1	NNPDF3.0NNLO	Sherpa 2.2.1	Default	NLO$^{(\ddagger)}$
$t\bar{t}W$	Sherpa 2.2.8	NNPDF3.0NNLO	Sherpa 2.2.8	Default	NLO$^{(\ddagger)}$
Vector boson + jets					
W+jets	Sherpa 2.2.1	NNPDF3.0NNLO	Sherpa 2.2.1	Default	NNLO
Z+jets	Sherpa 2.2.1	NNPDF3.0NNLO	Sherpa 2.2.1	Default	NNLO
Diboson					
WW	Sherpa 2.2.1	NNPDF3.0NNLO	Sherpa 2.2.1	Default	NLO$^{(\ddagger)}$
WZ	Sherpa 2.2.1	NNPDF3.0NNLO	Sherpa 2.2.1	Default	NLO$^{(\ddagger)}$
ZZ	Sherpa 2.2.1	NNPDF3.0NNLO	Sherpa 2.2.1	Default	NLO$^{(\ddagger)}$
Single Higgs boson					
ggF	Powheg-Box v2	NNPDF3.0NLO	Pythia 8.212	AZNLO	N3LO(QCD)+NLO(EW)
VBF	Powheg-Box v2	NNPDF3.0NLO	Pythia 8.212	AZNLO	NNLO(QCD)+NLO(EW)
$qq \to WH$	Powheg-Box v2	NNPDF3.0NLO	Pythia 8.212	AZNLO	NNLO(QCD)+NLO(EW)
$qq \to ZH$	Powheg-Box v2	NNPDF3.0NLO	Pythia 8.212	AZNLO	NNLO(QCD)+NLO(EW)$^{(\dagger)}$
$gg \to ZH$	Powheg-Box v2	NNPDF3.0NLO	Pythia 8.212	AZNLO	NLO+NLL
$t\bar{t}H$	Powheg-Box v2	NNPDF3.0NLO	Pythia 8.230	A14	NLO

Full run2 data results for non-resonant HH→bbττ

Uncertainty source	Non-resonant HH	Resonant $X \to HH$ 300 GeV	Resonant $X \to HH$ 500 GeV	Resonant $X \to HH$ 1000 GeV
Data statistical	81%	75%	89%	88%
Systematic	59%	66%	46%	48%
$t\bar{t}$ and $Z+$HF normalisations	4%	15%	3%	3%
MC statistical	28%	44%	33%	18%
Experimental				
Jet and $E_{\mathrm{T}}^{\mathrm{miss}}$	7%	28%	5%	3%
b-jet tagging	3%	6%	3%	3%
$\tau_{\text{had-vis}}$	5%	13%	3%	7%
Electrons and muons	2%	3%	2%	1%
Luminosity and pileup	3%	2%	2%	5%
Theoretical and modelling				
Fake-$\tau_{\text{had-vis}}$	9%	22%	8%	7%
Top-quark	24%	17%	15%	8%
$Z(\to \tau\tau)+$HF	9%	17%	9%	15%
Single Higgs boson	29%	2%	15%	14%
Other backgrounds	3%	2%	5%	3%
Signal	5%	15%	13%	34%

Full run2 data results for non-resonant HH→bbττ

Variable	$\tau_{\text{had}}\tau_{\text{had}}$	$\tau_{\text{lep}}\tau_{\text{had}}$ SLT	$\tau_{\text{lep}}\tau_{\text{had}}$ LTT
m_{HH}	✓	✓	✓
$m_{\tau\tau}^{\text{MMC}}$	✓	✓	✓
m_{bb}	✓	✓	✓
$\Delta R(\tau,\tau)$	✓	✓	✓
$\Delta R(b,b)$	✓	✓	
$\Delta p_{\text{T}}(\ell,\tau)$		✓	✓
Sub-leading b-tagged jet p_{T}		✓	
m_{T}^{W}		✓	
$E_{\text{T}}^{\text{miss}}$		✓	
$\mathbf{p}_{\text{T}}^{\text{miss}}$ ϕ centrality		✓	
$\Delta\phi(\tau\tau,bb)$		✓	
$\Delta\phi(\ell,\mathbf{p}_{\text{T}}^{\text{miss}})$			✓
$\Delta\phi(\ell\tau,\mathbf{p}_{\text{T}}^{\text{miss}})$			✓
S_{T}			✓

Full run2 data results for non-resonant HH→bbττ

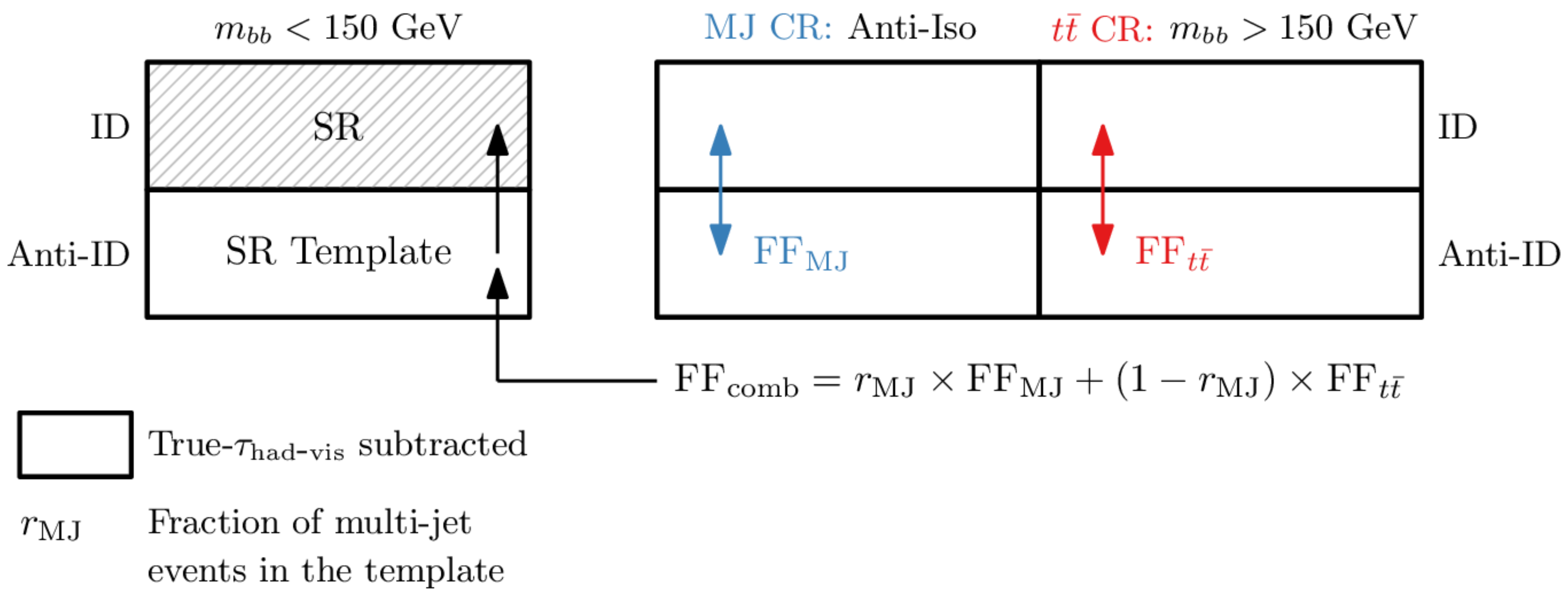

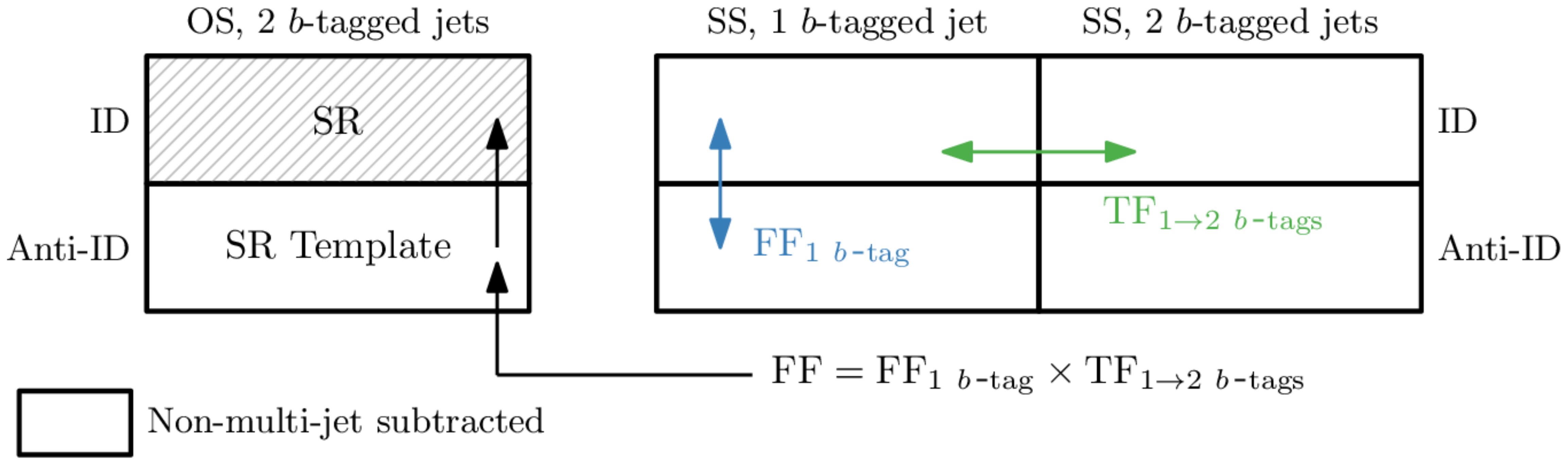

Schematic depiction of the combined fake-factor method used to estimate multi-jet and $t\bar{t}$ backgrounds with fake-$\tau_{\text{had-vis}}$ in the $\tau_{\text{lep}}\tau_{\text{had}}$ channel. Backgrounds which are not from events with fake-$\tau_{\text{had-vis}}$ originating from jets are estimated from simulation and are subtracted from data in all control regions. Events in which an electron or a muon is misidentified as a $\tau_{\text{had-vis}}$ are also subtracted, but their contribution is very small. Both sources are indicated by "True-$\tau_{\text{had-vis}}$ subtracted" in the legend.

Schematic depiction of the combined fake-factor method to estimate the multi-jet background with fake-$\tau_{\text{had-vis}}$ in the $\tau_{\text{had}}\tau_{\text{had}}$ channel. Backgrounds with true-$\tau_{\text{had-vis}}$ that are not from multi-jet events are simulated and subtracted from data in all the control regions. This is indicated by "Non-multi-jet subtracted" in the legend.

Full run2 data results for non-resonant HH→bbττ

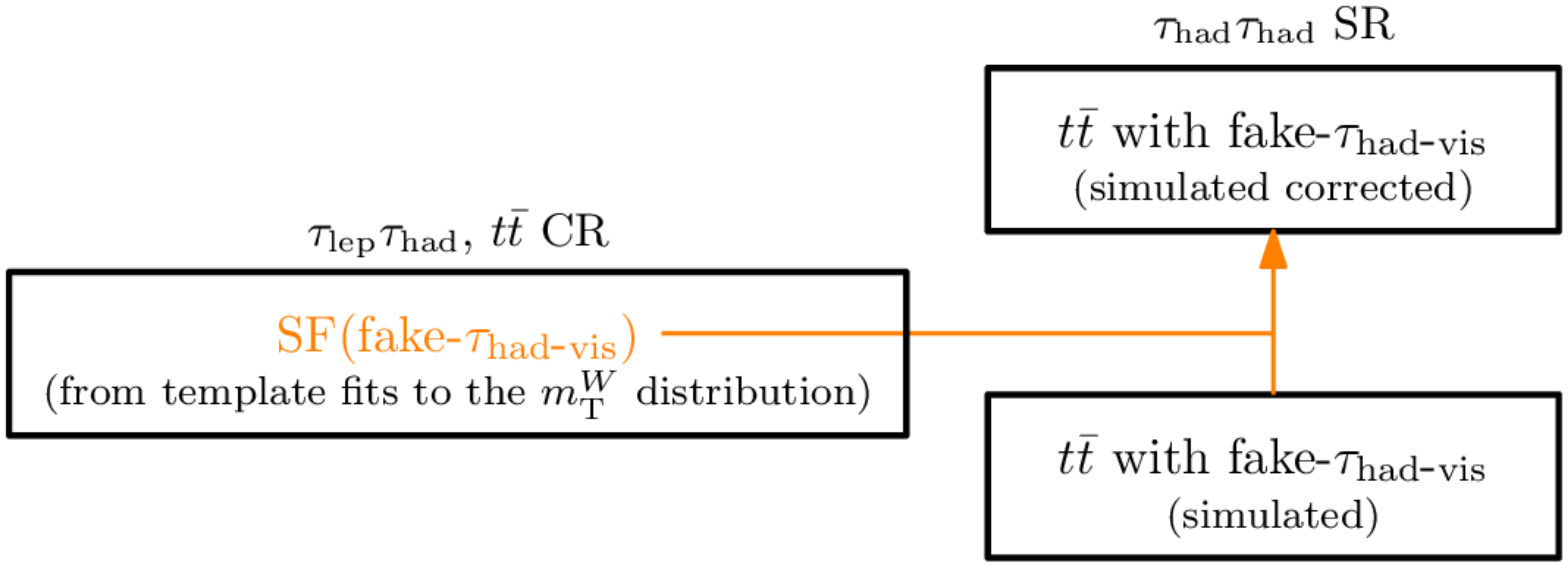

Schematic depiction of the fake-$\tau_{\text{had-vis}}$ scale-factor method to estimate the $t\bar{t}$ background with fake-$\tau_{\text{had-vis}}$ in the $\tau_{\text{had}}\tau_{\text{had}}$ channel.

Full run2 data results for non-resonant HH→bbγγ

4 signal region categories
That are defined by $m_{bb\gamma\gamma}$ and BDT output
targeting the SM HH signal and BSM signals with varied k_λ

- Two HH mass categories:
  1. Low mass
  2. High mass

- One BDT trained in each mass region, on BSM signal with $k_\lambda = 10$ for low mass and on SM signal with $k_\lambda = 1$ for high mass

- Two BDTs categories:
  - BDT-tight and BDT-loose, in each of the two mass categories

arXiv:2112.11876

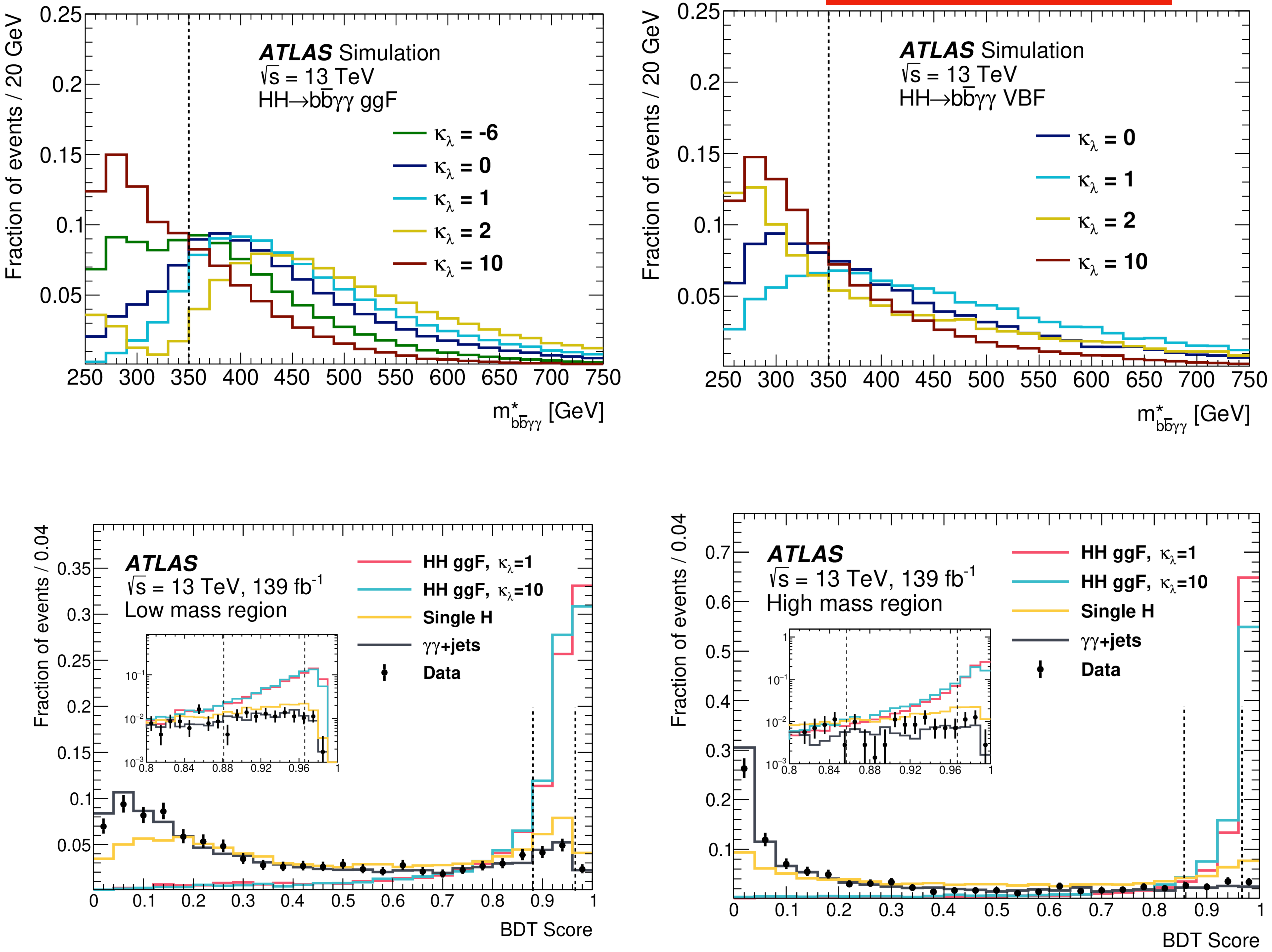

Full run2 data results for non-resonant HH→bbγγ

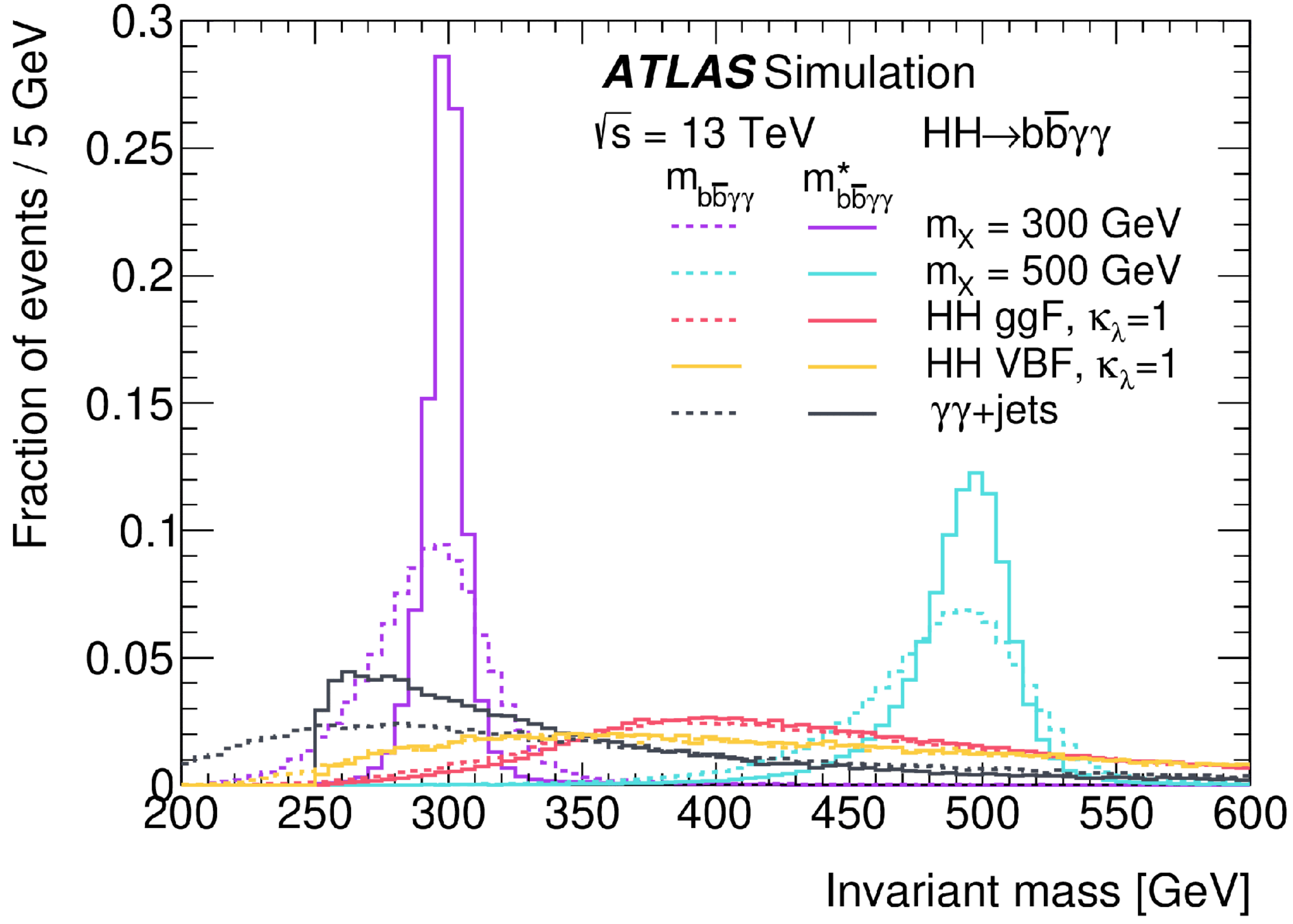

Reconstructed four-body mass for m_X = 300 GeV and m_X = 500 GeV resonant signal benchmarks, for the SM HH production processes and for the γγ+jets background. Dashed lines represent the distribution of $m_{b\bar{b}\gamma\gamma}$ while solid lines represent the distribution of $m^*_{b\bar{b}\gamma\gamma}$. Distributions are normalized to unit area.

Full run2 data results for non-resonant HH→bbγγ

Table 3: Definition of the categories used in the HH nonresonant search. Before entering the BDT-based categories, events are required to satisfy the common preselection.

Category	Selection criteria
High mass BDT tight	$m^*_{b\bar{b}\gamma\gamma} \geq 350$ GeV, BDT score $\in [0.967, 1]$
High mass BDT loose	$m^*_{b\bar{b}\gamma\gamma} \geq 350$ GeV, BDT score $\in [0.857, 0.967]$
Low mass BDT tight	$m^*_{b\bar{b}\gamma\gamma} < 350$ GeV, BDT score $\in [0.966, 1]$
Low mass BDT loose	$m^*_{b\bar{b}\gamma\gamma} < 350$ GeV, BDT score $\in [0.881, 0.966]$